Materials Today Bio 22 (2023) 100749

Contents lists available at ScienceDirect

Materials Today Bio

journal homepage: www.journals.elsevier.com/materials-today-bio

Bi-lineage inducible and immunoregulatory electrospun fibers scaffolds for synchronous regeneration of tendon-to-bone interface

Haihan Gao [a,b,1], Liren Wang [a,b,1], Zhiqi Lin [a], Haocheng Jin [a], Yangbao Lyu [a], Yuhao Kang [a], Tonghe Zhu [e], Jinzhong Zhao [a,c,d,*], Jia Jiang [a,c,**]

[a] Department of Sports Medicine, Shanghai Sixth People's Hospital Affiliated to Shanghai Jiao Tong University School of Medicine, Shanghai, 200233, China
[b] Regenerative Sports Medicine and Translational Youth Science and Technology Innovation Workroom, Shanghai Jiao Tong University School of Medicine, No. 227 South Chongqing Road, Shanghai, 200025, China
[c] Regenerative Sports Medicine Lab of the Institute of Microsurgery on Extremities, Shanghai Sixth People's Hospital Affiliated to Shanghai Jiao Tong University School of Medicine, Shanghai, 200233, China
[d] Shanghai Engineering Research Center for Orthopaedic Material Innovation and Tissue Regeneration Building 3, Langu Science and Technology Park, Lane 70, Haiji 6th Road, Shanghai, 201306, China
[e] School of Chemistry and Chemical Engineering, Shanghai Engineering Research Center of Pharmaceutical Intelligent Equipment, Shanghai Frontiers Science Research Center for Druggability of Cardiovascular Non-coding RNA, Institute for Frontier Medical Technology, Shanghai University of Engineering Science, 333 Longteng Rd., Shanghai, 201620, PR China

ARTICLE INFO

Keywords:
Rotator cuff tear
Tendon-to-bone interface
Bioactive ions
Macrophages
Mesoporous bioglass nanoparticles
Electrospinning

ABSTRACT

Facilitating regeneration of the tendon-to-bone interface can reduce the risk of postoperative retear after rotator cuff repair. Unfortunately, undesirable inflammatory responses following injury, difficulties in fibrocartilage regeneration, and bone loss in the surrounding area are major contributors to suboptimal tendon-bone healing. Thus, the development of biomaterials capable of regulating macrophage polarization to a favorable phenotype and promoting the synchronous regeneration of the tendon-to-bone interface is currently a top priority. Here, strontium-doped mesoporous bioglass nanoparticles (Sr-MBG) were synthesized through a modulated sol-gel method and Bi-lineage Inducible and Immunoregulatory Electrospun Fibers Scaffolds (BIIEFS) containing Sr-MBG were fabricated. The BIIEFS were biocompatible, showed sustained release of multiple types of bioactive ions, enhanced osteogenic and chondrogenic differentiation of mesenchymal stem cells (MSCs), and facilitated macrophage polarization towards the M2 phenotype *in vitro*. The implantation of BIIEFS at the torn rotator cuff resulted in greater numbers of M2 macrophages and the synchronous regeneration of tendon, fibrocartilage, and bone at the tendon-to-bone interface, leading to a significant improvement in the biomechanical strength of the supraspinatus tendon-humerus complexes. Our research offers a feasible strategy to fabricate immunoregulatory and multi-lineage inducible electrospun fibers scaffolds incorporating bioglass nanoparticles for the regeneration of soft-to-hard tissue interfaces.

1. Introduction

Following surgical repair for rotator cuff tear (RCT), a considerable proportion of patients, ranging from 20% to 94%, may encounter retear, leading to significant impairment of the mobility of the shoulder joint [1]. The inability to restore the native structure and function of the tendon-to-bone interface contributes significantly to postoperative retear [2,3]. The tendon-to-bone interface is a complex structure that connects tendon and bone, and its primary function is to transmit stress and reduce excessive stress concentration [4]. The function of the tendon-to-bone interface is closely related to its unique structure which is comprised of four distinct and diverse layers, which include the

* Corresponding author. Department of Sports Medicine, Shanghai Sixth People's Hospital Affiliated to Shanghai Jiao Tong University School of Medicine, Shanghai, 200233, China.
** Corresponding author. Department of Sports Medicine, Shanghai Sixth People's Hospital Affiliated to Shanghai Jiao Tong University School of Medicine, Shanghai, 200233, China.
E-mail addresses: jzzhao@sjtu.edu.cn (J. Zhao), jessicajj19@sjtu.edu.cn (J. Jiang).
[1] Haihan Gao and Liren Wang contributed equally to this work.

https://doi.org/10.1016/j.mtbio.2023.100749
Received 27 April 2023; Received in revised form 18 July 2023; Accepted 25 July 2023
Available online 26 July 2023

tendon layer, uncalcified fibrocartilage layer, calcified fibrocartilage layer, and bone layer [5,6]. Unfortunately, even with surgical repair, the fibrocartilage layers of the tendon-to-bone interface cannot regenerate and are replaced by fibrous scar tissue [7,8]. Scar tissue does not possess the normal function of the tendon-to-bone interface, leading to a significantly increased chance of retear [9]. In addition, the loss of mechanical loading and increased osteoclast activity can lead to bone loss around the tendon-to-bone interface, which is closely related to poor tendon-bone healing [7,10,11]. Thus, it is imperative to promote synchronous regeneration of different layers at the tendon-to-bone interface to achieve optimal healing.

Dysregulated and chronic inflammatory response resulting from an imbalance between pro-inflammatory M1 and anti-inflammatory M2 macrophages after tendon-to-bone interface injuries is one of the potential causes of problematic fibrocartilage regeneration and surrounding bone loss [12,13]. In the early stages of an RCT, there is a predominance of pro-inflammatory M1 macrophages that secrete large amounts of inflammatory factors such as interleukin-1β (IL-1β), interleukin-6 (IL-6), and tumor necrosis factor-α (TNF-α) [14]. Excessive secretion of inflammatory factors can both inhibit the regeneration of the fibrocartilage layer and enhance the activity of osteoclasts [13]. Unfortunately, the numbers of M2 macrophages, which are responsible for expediting the resolution of inflammation and promoting tissue regeneration, are insufficient to support the regeneration of the fibrocartilage and bone during the tendon-bone healing process [13]. Therefore, modulation of macrophage polarization to the favorable M2 phenotype during the tendon-bone healing process is a feasible method for the amelioration of aberrant inflammatory responses and the promotion of the regeneration of the tendon-to-bone interface [13,15,16].

Mesoporous bioactive glass has immunoregulatory properties and can induce effective tissue regeneration through the incorporation of bioactive elements [17–19]. Zheng et al. successfully prepared mesoporous bioactive glass nanoparticles incorporating cerium (Ce-MBGNs) through a post-impregnation strategy [20]. The Ce-MBGNs were found to reduce the expression of inflammation-related genes in activated macrophages and promote the expression of osteogenic-related genes in osteoblast-like SAOS-2 cells [20]. Strontium (Sr) is a versatile bioactive element and its incorporation in bioactive glass can enhance the bioactivity and enrich the biological functions of bioactive glass [21]. Zhao et al. synthesized Sr-containing bioactive glass microspheres (SrBGM) and found that SrBGM could accelerate early vascularization during bone regeneration by promoting M2 polarization of macrophages [22]. Cai et al. prepared an injectable hydrogel loaded with strontium-doped bioglass (SrBG) [23]. The SrBG acted as a hydrogel crosslinker and released strontium ions continuously, which promoted the chondrogenic differentiation of mesenchymal stem cells and the M2 polarization of macrophages [23]. The injectable hydrogel loaded with SrBG was found to inhibit macrophage-mediated inflammation and promote cartilage regeneration [23]. Mesoporous bioactive glasses (MBG) doped with bioactive elements hold significant potential for the regeneration of both soft and hard tissue. However, whether strontium-doped MBG can regulate the inflammatory response and promote the synchronous regeneration of the tendon-to-bone interface remains unknown.

In our previous study, we prepared lithium-containing mesoporous silica and loaded it into electrospun fibers scaffolds using electrospinning [24]. These electrospun fibers scaffolds exhibited sustained release of lithium ions, which activated the Wnt/β-catenin pathway to promote bone regeneration at the tendon-to-bone interface [24]. However, neither the significance of fibrocartilage regeneration at the tendon-to-bone interface nor the adverse impact of inflammatory responses on tendon-bone healing were considered in the study. To better meet the requirements of synchronous tissue regeneration at the tendon-to-bone interface and promote macrophages polarize to favorable phenoytpe for tissue regeneration, a novel Sr-MBG was synthesized and incorporated into electrospun fibers via electrospinning to create bi-lineage inducible and immunoregulatory electrospun fibers scaffolds (Fig. 1). We hypothesized that the release of Sr-MBG and various bioactive ions from the BIIEFS could stimulate osteogenic and chondrogenic differentiation of mesenchymal stem cells and regulate macrophage polarization *in vitro*. Histological experiments, micro-computed tomography (micro-CT), and biomechanical tests were conducted to evaluate whether BIIEFS could modulate the polarization of local macrophages and enhance the synchronous regeneration of different layers of the tendon-to-bone interface *in vivo*.

2. Materials and methods

2.1. Reagents and materials

Cetyltrimethylammonium bromide (CTAB), triethanolamine, tetraethyl silicate (TEOS), triethyl phosphate (TEP), calcium nitrate tetrahydrate ($Ca(NO_3)_2{\cdot}4H_2O$), strontium nitrate ($Sr(NO_3)_2$), and gelatin were purchased from Sigma-Aldrich (St Louis, MO, USA). The synthesis of Poly (ester urethane) urea (PEUU) was performed as previously described [25]. 1,1,1,3,3,3-hexafluoro-2-propanol (HFIP) was obtained from Chembee (Shanghai, China). Dulbecco's Modified Eagle Medium (DMEM), Minimum Essential Medium α (α-MEM), phosphate-buffered saline (PBS), penicillin-streptomycin, trypsin, cell culture freezing medium, and 4,6-diamidino-2-phenylindole (DAPI) were bought from Gibco (Waltham, MA, USA). Lipopolysaccharide (LPS), Interleukin 4 (IL-4), and Interleukin 13 (IL-13) were bought from Yeasen (Shanghai, China). Cell Counting Kit-8 (CCK-8), Calcein/Propidium Iodide (AM/PI) cell viability/cytotoxicity Assay Kit, Alizarin Red Staining solution, Alkaline Phosphatase Assay Kit, and the Modified Oil Red O Staining Kit were bought from Beyotime (Shanghai, China). Cetylpyridinium chloride was purchased from Sigma-Aldrich. Osteogenic and chondrogenic differentiation induction mediums were purchased from Cyagen (Shanghai, China). EZ-press RNA Purification Kit, 2 × SYRB Green qPCR Master Mix, and 4 × Reverse Transcription were acquired from EZBioscience (Roseville, MN, USA). Picrosirius red solution kit was purchased from Solarbio (Beijing, China).

2.2. Preparation of MBG and Sr-MBG

A modulated sol-gel method was employed to synthesize Mesoporous Bioglass Nanoparticles (MBG) and Sr-MBG. In brief, 2 g of CTAB and 0.08 g of triethanolamine were dispersed in 20 mL of ultrapure water and agitated vigorously for 1 h at 95 °C. After that, 1.5 mL of TEOS was added dropwise to the solution and stirred for 1 h before the addition of 0.03 mol $Ca(NO_3)_2{\cdot}4H_2O$, 0.03 mol $Sr(NO_3)_2$, and 0.01 mol TEP with constant stirring for 1 h. The precipitate was collected and washed with ethanol and ultrapure water. It was then dried in an oven before being transported to a muffle furnace to calcine at 650 °C for 3 h, finally yielding Sr-MBG. The procedure for MBG synthesis was similar to that of Sr-MBG, except for the addition of $Sr(NO_3)_2$.

2.3. Fabrication of electrospun fibers scaffolds

The process of electrospinning was utilized to fabricate scaffolds composed of electrospun fibers. Solution 1 was prepared by dissolving 1.2 g of PEUU in HFIP to yield a 12% (w/v) solution with a total volume of 10 mL. After that, HFIP was used to dissolve PEUU and gelatin (75:25) to create 10 mL of 12% (w/v) solution 2. Subsequently, 100 mg of Sr-MBG was introduced into solution 2 and agitated until the particles were uniformly dispersed throughout the solution, to yield solution 3. The PEUU electrospun fibers scaffolds (EFS) and PEUU/gelatin electrospun fibers scaffolds (EFS1) were fabricated through electrospinning of solutions 1 and 2, respectively. After ultrasonically treated for 1 h prior to electrospinning, solution 3 was electrospun to fabricate bi-lineage inducible and immunoregulatory electrospun fibers scaffolds (BIIEFS). All electrospinning operations were conducted with the

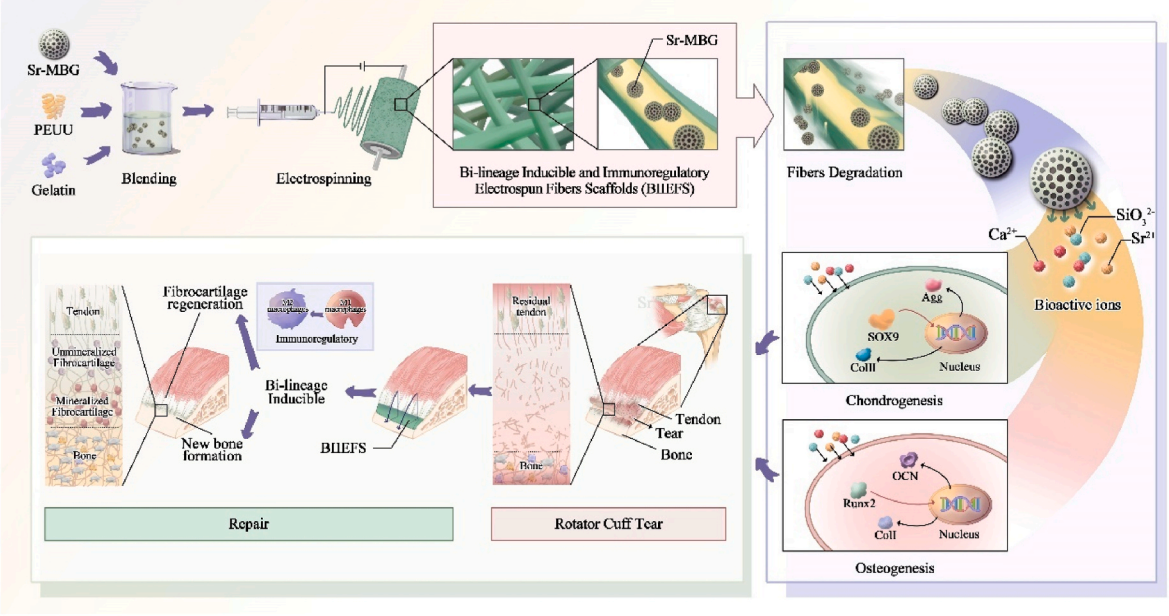

Fig. 1. Schemata of fabrication of Bi-lineage Inducible and Immunoregulatory Electrospun Fibers Scaffolds (BIIEFS) for synchronous regeneration of tendon-to-bone interface. Electrospinning was used to fabricate BIIEFS that were capable of the sustained release of numerous bioactive ions. BIIEFS enhanced chondrogenesis and osteogenesis of BMSCs and possessed immunoregulatory properties. The in situ implantation of BIIEFS for rotator cuff tears accelerated anti-inflammatory M2 macrophage polarization and promoted synchronous regeneration of soft and hard tissue of the tendon-to-bone interface.

following parameters: an applied voltage of 12 kV, a syringe needle tip-to-collector distance of 15 cm, a flow rate of 1 mL/h, an ambient temperature of 25 °C, and a relative humidity of 25 ± 5%.

2.4. Characterizations of MBG, Sr-MBG, and electrospun fibers scaffolds

Scanning electron microscopy (SEM, RISE-MANGA, Czech Republic) and transmission electron microscopy (TEM, TALOS F200X, USA) were utilized to examine the microstructures and nanostructures of the Sr-MBG and electrospun fibers scaffolds. ImageJ software (NIH, USA) was used to measure the average diameters of the MBG, Sr-MBG, and electrospun fibers scaffolds. The contact angle of water was evaluated by DSA100 (KrüssGmbH, Germany). Material testing equipment (Instron 5969, USA) was used to determine the mechanical properties of the electrospun fibers scaffolds. The porosity of the electrospun fibers scaffolds was measured with ImageJ. Fourier-transform infrared (FTIR) spectroscopy was performed with an infrared spectrometer (Nicolet 6700, Thermo Fisher Scientific, USA) in absorption mode at 2 cm^{-1} intervals in the wavelength range 400–4000 cm^{-1}. X-ray photoelectron spectroscopy (XPS, AXIS UltraDLD, China) was used to determine the elemental composition and valence distribution of MBG and Sr-MBG.

2.5. Release of ions and degradation of electrospun fibers scaffolds

Electrospun fibers scaffolds measuring 1 × 1 cm^2 were immersed in 2 mL of PBS (pH = 7.4) for 1, 3, 5, 7, 14, 21, or 28 days. The concentrations of Sr, Ca, and Si in the supernatants were then determined using an inductively coupled plasma emission spectrometer (ICP-OES, Avio500, PerkinElmer, Singapore). The degradation of the electrospun fibers scaffolds was determined with lipase in PBS. The electrospun fibers scaffolds were cut in a circle with a 20-mm diameter, weighed (W_0), and immersed in 3 mL of PBS at 37 °C. At 1, 3, 7, 14, 21, and 28 days, the electrospun fibers scaffolds were removed from the PBS and rinsed with deionized water. The final weight (Wt) was calculated after lyophilization. The remaining weight of the electrospun fibers scaffolds at different time points was calculated using the equation: Remaining mass (%) = $Wt/W_0 \times 100$.

2.6. Identification of BMSCs and tri-lineage differentiation

Rat bone marrow-derived stem cells (BMSCs) were bought from Pricella (Wuhan, China). Flow cytometry was used to identify positive (CD90 and C44) and negative (CD34 and CD45) surface markers. Section S1.1 of the ESM included the flow cytometry experimental details.

The BMSCs were induced to undergo osteogenic, adipogenic, and chondrogenic differentiation in specific induction media (Cyagen, China). The tri-lineage differentiation of the BMSCs was verified using Alizarin Red, Oil Red, and Alcian Blue staining.

The outcomes of the identification of positive and negative surface markers of BMSCs and their tri-lineage differentiation are presented in Section S2 of the ESM.

2.7. Cytocompatibility of electrospun fibers scaffolds

The cytocompatibility of the electrospun fibers scaffolds was evaluated *in vitro* using AM/PI, cytoskeletal staining, and CCK-8 assays. After sterilization, the electrospun fibers scaffolds were placed in 24-well plates and 1.0 × 10^4 BMSCs were seeded on each scaffold. The cells were cultured for 1, 3, and 5 days on the scaffolds before the addition of the CCK-8 working solution and incubation at 37 °C for 1 h. The working solution was then transferred to 96-well plates and the absorbance at 450 nm was measured using an automatic microplate reader (MPR-A9600, Thomas Scientific, USA). The seeded cells were subjected to AM/PI staining at two time points, specifically, on days 1 and 5 post-seeding. Confocal laser scanning microscopy (Leica TCS SP8, Leica, Germany) was used to observe the cells, which were stained green for living cells and red for dead cells, allowing the calculation of the cell live-dead ratio. The cell cytoskeleton and nucleus were stained with phalloidin and DAPI, respectively, and evaluated under confocal laser scanning microscopy.

2.8. In vitro cell induction

To determine the prospective effects of the electrospun fibers scaffolds on osteogenesis and chondrogenesis of BMSCs, EFS1 and BIIEFS were soaked for two weeks in osteogenic and chondrogenic induction

medium at a ratio of 100 cm^2/20 mL to obtain the extract induction medium. The osteogenic and chondrogenic effect of the extract induction medium was then evaluated on BMSCs.

2.8.1. Osteogenic induction

BMSCs (1.0×10^7) were seeded in 6-well tissue culture plates and cultured for 14 days in the osteogenic extract induction medium. Reverse transcription-quantitative polymerase chain reaction (RT-qPCR) and western blotting (WB) were used to assess the expression of osteogenic marker genes. BMSCs (5.0×10^4) were seeded in 24-well plates and cultured for 7 and 14 days in an osteogenic extract induction medium. Osteogenesis was evaluated using Alizarin Red Staining (ARS), Alkaline Phosphatase Staining (ALP), and immunofluorescent staining. Following ARS staining, the calcium deposits in BMSCs were dissolved in a cetylpyridinium chloride solution for 2 h at ambient temperature. The absorbance of the eluate was measured at 565 nm in a microplate reader (MPR-A9600, Thomas Scientific, USA). ALP activity was measured using an Alkaline Phosphatase Assay Kit (Beyotime, China), following the provided protocol.

2.8.2. Chondrogenic induction

BMSC pellets were used to investigate the effect of various chondrogenic extract induction mediums on chondrogenic induction, with reference to a previous report [26]. Following three weeks, the pellets underwent sectioning for Alcian blue, Safranin-O staining, and collagen II immunohistochemistry. The volume of pellets was calculated as described previously [26]. The Bern score was employed to assess the chondrogenesis of cell pellets [27]. 1.0×10^7 BMSCs were seeded in 6-well tissue culture plates and cultured for 21 days in a chondrogenic extract induction medium. After 3 weeks, the expression of chondrogenic markers was measured using RT-qPCR and WB. 5.0×10^4 BMSCs were seeded on 24-well tissue culture plates and subjected to a 21 days culture period in the presence of a chondrogenic extract induction medium. To assess the expression of chondrogenic marker protein, immunofluorescent staining was performed. Section S1.1 of the ESM contains a detailed description of the RT-qPCR, WB, and immunofluorescence.

We furthur evaluated the potential effect of the extract of EFS1 and BIIEFS on tenogenesis of tendon-derived stem cells (TDSCs). Methods are described in detail in Section S1.1 of the ESM.

2.9. Macrophage polarization experiments

RAW 264.7 cells were bought from Pricella (China). The extract medium was obtained by soaking EFS1 and BIIEFS in DMEM at a ratio of 100 cm^2/20 mL for 2 weeks. The effect of the extract medium on the polarization of macrophages M1 and M2 was evaluated.

RAW 264.7 cells (1.0×10^6) were seeded in 6-well plates and cultured in DMEM, EFS1 extract medium, or BIIEFS extract medium. LPS (200 ng/mL) was added to the cultures and incubated for 48 h to induce macrophage M1 polarization. M2 macrophage polarization was induced by incubation with 10 ng/mL of IL-4 and IL-13. Macrophage polarization was evaluated by immunofluorescence staining, flow cytometry, and RT-qPCR. The details of these procedures are described in Section S1.1 of the ESM.

2.10. In vivo experiments

2.10.1. Establishment of rat RCT model

All animal experimentation was approved and supervised by the Institutional Animal Care and Use Committee (IACUC) of Shanghai Sixth People's Hospital Affiliated with the Shanghai Jiao Tong University School of Medicine (Animal Experiment Registration number: DWSY2021-0113). A total of 128 mature male rats weighing 250 g ± 50 g were used. The rats were randomly divided into four groups: 1) Defect group; 2) Simple repair group; 3) EFS1 repair (EFS1 group); 4) BIIEFS repair (BIIEFS group). Briefly, the right supraspinatus tendon was detached from the humerus and subsequently reattached to its original imprint area using a transosseous suture. The details of the surgical procedure are described in Section S1.2 of the ESM. Six rats were sacrificed at 4 and 8 weeks for histological, immunohistochemical, and Micro-CT evaluations, while four rats were sacrificed for the biomechanical test.

2.10.2. Histology and immunohistochemistry (IHC) staining

The supraspinatus tendon-humerus complexes were fixed in 10% formalin for three days, followed by one month of decalcification. After dehydration and embedding, 4-μm serial sections were cut and stained with hematoxylin and eosin (HE), Safranin O/Fast Green, toluidine blue, collagen II immunohistochemistry, and CD206 immunohistochemistry. The sections were evaluated and imaged using a Leica DM4000B microscope (Germany). A semiquantitative evaluation of the regenerative tendon-to-bone interface was then performed using a histological scoring system and tendon-maturing score [28,29]. The details of the histological scoring system and tendon-maturing score are described in Section S1.3 and S1.4 of the ESM. ImageJ software was used to calculate the relative positive areas of the immunohistochemistry images.

2.10.3. Microcomputed tomography (Micro-CT) analysis

Micro-CT (eXplore Locus SP, Canada) was used to assess the bone mineral density (BMD) and bone volume/total volume (BV/TV) of the greater tubercles. Each specimen was scanned using 270 mA, 90 kV, and a voxel size of 18 μm. For three-dimensional reconstruction, CTVox software (USA) was used. The tendon-humerus complex footprint was selected as the region of interest. The software SkyScan CT Analyzer (Bruker, Germany) was used to assess the BMD and BV/TV of each specimen.

2.10.4. Biomechanical test

After harvesting the supraspinatus tendon–humerus complexes from the experimental rats, the cross-sectional area of the tendon at the tendon-to-bone interface was measured using a digital caliper (Tajima). The biomechanical measurements were conducted using an Instron 5569 universal testing machine. The supraspinatus tendon was immobilized with a clamp, while the proximal humerus was immobilized with a second clamp (Fig. S2(a)). The evaluation of all supraspinatus tendon-humerus complexes was conducted following previously established protocols [30]. Rupture of the supraspinatus tendon–humerus complexes during the procedure indicated completion of the test. Load-strain curves were plotted to determine the failure load, stiffness, and stress.

2.11. Statistical analysis

The experimental data were analyzed and visualized using SPSS 21 (IBM, USA) and Origin 2021 (USA) software. The levels of significance were $^*P < 0.05$, $^{**}P < 0.01$, and $^{***}P < 0.001$.

3. Results

3.1. Characterization of MBG and Sr-MBG

The schematic diagram for the synthesis of Sr-MBG is depicted in Fig. 2(a). The micro and nano morphology of MBG and Sr-MBG were examined using SEM and TEM, as illustrated in Fig. 2(b) and (c). Sr-MBG had a more regular spherical shape, smoother surfaces, and evenly distributed pores than MBG. MBG had a diameter of 100.54 ± 15.73 nm, whereas Sr-MBG had a diameter of 40.40 ± 4.14 nm (Fig. 2(d)). Sr-MBG was dispersed in the electrospun fibers without evident morphological changes (Fig. 2(e)). The wide-scan XPS results of MBG and Sr-MBG are shown in Fig. 2(f) and (g). The narrow scan revealed that MBG contained Si and Ca but not Sr (Fig. 2(h)). The narrow scan of the Sr-MBG revealed Si 2p, Ca 2p, and Sr 3d changes in binding energy, indicating that the Sr-MBG contained Si, Ca, and Sr elements (Fig. 2(i)). Energy dispersive

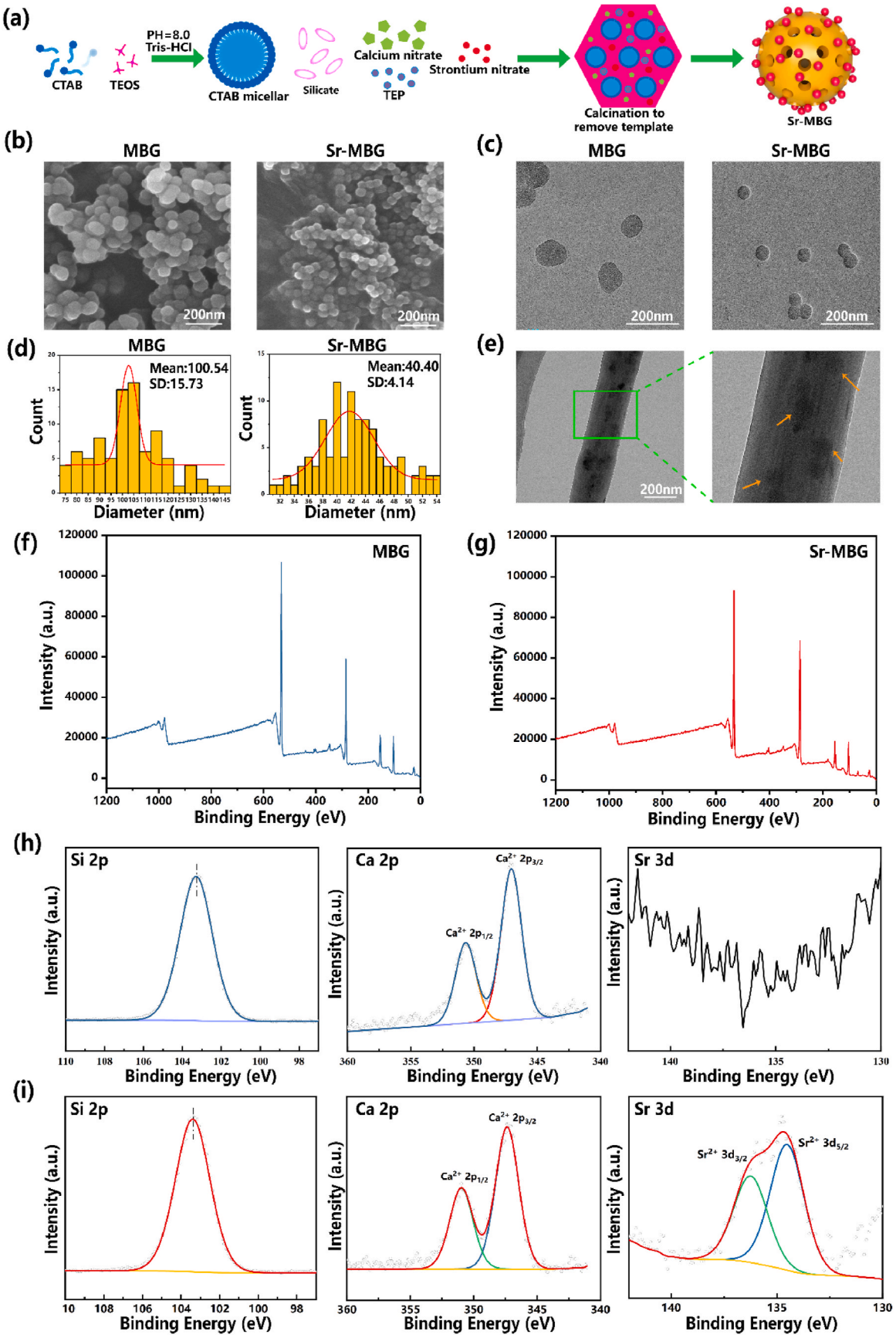

Fig. 2. Characterization of MBG and Sr-MBG. (a) Schematic diagram showing the synthesis of strontium-doped bioglass nanoparticles. (b) SEM images of MBG and Sr-MBG. (c) TEM images of MBG and Sr-MBG. (d) The average diameters of MBG and Sr-MBG. (e) TEM images of Sr-MBG in electrospun fibers scaffolds. Orange arrow: Sr-MBG in electrospun fibers. (f)–(g) Wide-scan XPS of MBG and Sr-MBG. (h)–(i) Narrow scan of Si 2p, Ca 2p, and Sr 3d in MBG and Sr-MBG.

spectroscopy (EDS) was used to determine the elemental composition of MBG and Sr-MBG (Fig. S4(a) of the ESM). The distribution of Sr, Ca, and Si within the Sr-MBG was revealed by EDS mapping (Fig. S4(a) of the ESM). The results of XPS and EDS mapping demonstrated that strontium was effectively incorporated into mesoporous bioglass nanoparticles.

3.2. Characterization of electrospun fibers scaffolds

Fig. 3(a) depicts the micro morphology and average diameters of EFS, EFS1, and BIIEFS. All SEM images of the samples exhibited fibers with random orientations and three-dimensional porous structures. EFS had an average diameter of 0.99 ± 0.15 nm, while EFS1 had an average diameter of 1.47 ± 0.24 nm. The average diameter of BIIEFS was 1.46 ± 0.23 nm, and it appeared that the presence of Sr-MBG did not affect the diameter of the electrospun fibers. There were no appreciable differences in the porosities of EFS (84.45 ± 3.36%), EFS1 (77.37 ± 5.16%), and BIIEFS (74.56 ± 4.05%) (Fig. 3(b)). PEUU is a hydrophobic substance with electrospun fibers scaffolds that is unfavorable to cell spreading and proliferation [31]. Consequently, to enhance the hydrophilic properties of PEUU, a blend of gelatin and PEUU was utilized for the process of electrospinning. The water contact angle for EFS was found to be 124.35 ± 3.92°, while EFS1 exhibited a water contact angle of 47.35 ± 1.16°. The incorporation of Sr-MBG resulted in a further reduction in the water contact angle of BIIEFS (34.63 ± 2.38°), as evidenced by the data presented in Fig. 3(a) and (c).

Fig. 3(d) depicts the mechanical properties representative of EFS, EFS1, and BIIEFS. The values of Young's modulus, tensile strength, and elongation at break were determined by analyzing the strain-stress curves, as described earlier [24]. The Young's modulus values for EFS, EFS1, and BIIEFS were determined to be 11.40 ± 0.86 Mpa, 6.07 ± 0.24 Mpa, and 9.08 ± 0.26 Mpa, respectively. The incorporation of gelatin and Sr-MBG into the electrospun fibers resulted in a reduction of tensile stress. The tensile stress values for EFS, EFS1, and BIIEFS were determined to be 17.77 ± 1.04 Mpa, 11.88 ± 1.02 Mpa, and 8.24 ± 0.51 Mpa, respectively. The trend of elongation at rupture was comparable to the trend of tensile stress.

The FTIR spectra of the Sr-MBG, EFS, EFS1, and BIIEFS are shown in Fig. 3(e). The stretching vibration of O–H, which was abundant in the gelatin, was reflected by the broad peak between 3500 and 3300 cm^{-1}. The EFS1 and BIIEFS exhibited a prominent gelatin peak at 1570 cm^{-1}, which can be attributed to large numbers of N–H bonds. In comparison to EFS and EFS1, an additional peak at 1071 cm^{-1} was observed in

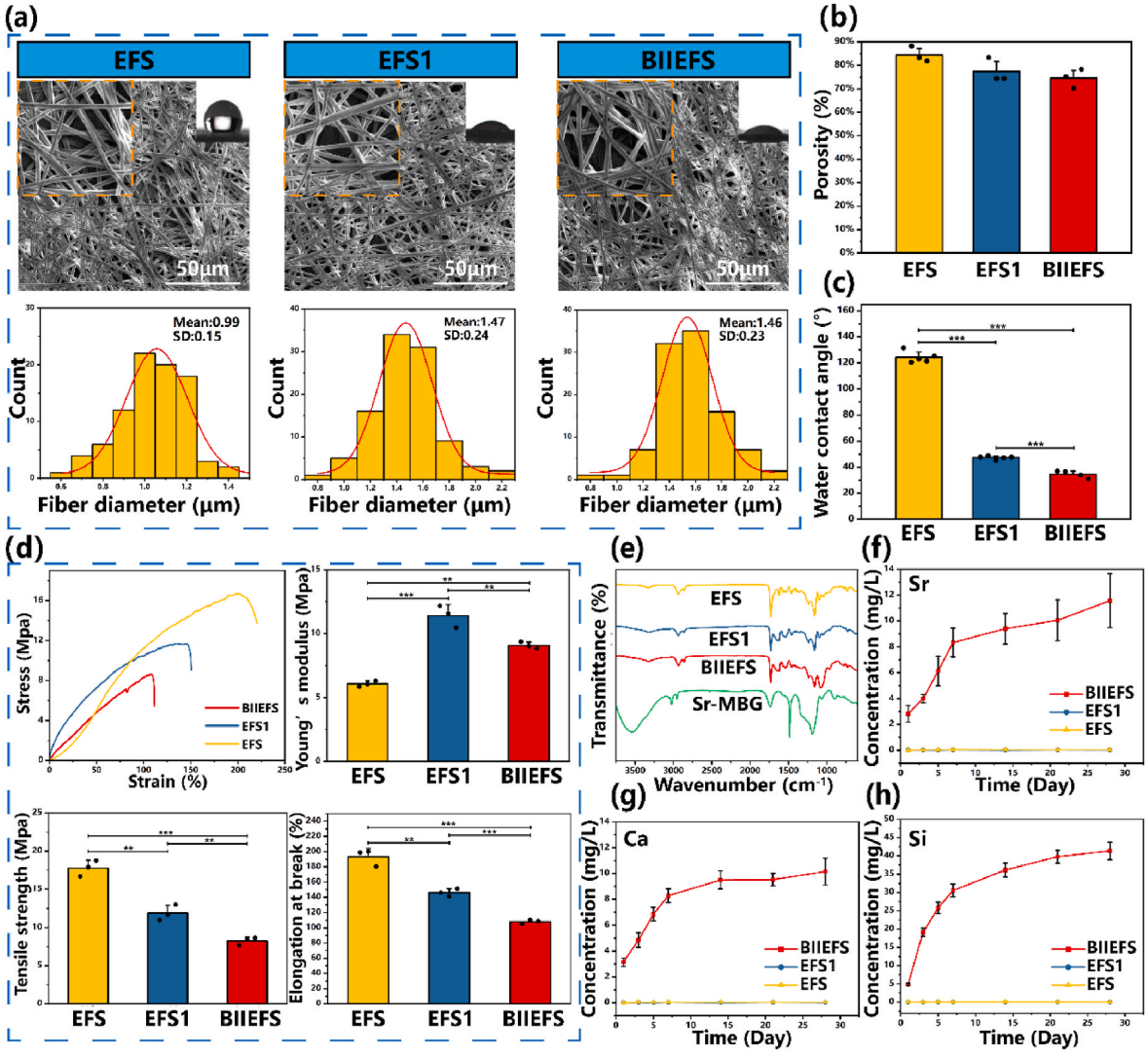

Fig. 3. Characterization of the electrospun fibers scaffolds. (a) SEM images and average diameters of EFS, EFS1, and BIIEFS. (b) The porosity of EFS, EFS1, and BIIEFS. (c) The water contact angles of EFS, EFS1, and BIIEFS. (d) Mechanical properties of electrospun fibers scaffolds: Stress-strain curves, Young's modulus, tensile strength, and elongation at break. (e) FTIR spectra of electrospun fibers scaffolds and Sr-MBG. (f)–(h) The ion release curves of Sr, Ca, and Si from EFS, EFS1, and BIIEFS. (**p < 0.01, and ***p < 0.001).

BIIEFS, corresponding to the stretching vibration of Si–*O*–Si. The incorporation of gelatin and Sr-MBG in BIIEFS was confirmed by the FTIR spectral data. Fig. 3(f), (g), and 3(h) show the curves of ion release for strontium, calcium, and silicon, respectively. It was observed that the rate of ion release was rapid during the first week but slowed considerably thereafter. At 28 days, ions were still being released, indicating that BIIEFS exhibited a controlled release behavior. We further evaluated the degradation of the electrospun fibers scaffolds in PBS *in vitro*. The EFS1 and BIIEFS exhibited faster degradation rates than EFS, which might be attributed to the addition of gelation and Sr-MBG (Fig. S5(a)). The SEM images revealed that during fibers degradation, the Sr-MBG in BIIEFS was exposed on the fibers surface, allowing for the continuous release of various bioactive ions (Figs. S5(b) and S5(c)).

3.3. Biocompatibility of electrospun fibers scaffolds

While PEUU and gelatin are biocompatible materials it remains to be determined whether BIIEFS is appropriate for cell proliferation. The biocompatibility of the electrospun fibers scaffolds was evaluated using live/dead staining, cytoskeletal staining, and CCK-8 assays. After 1 and 5 days of incubation, live/dead staining indicated that BMSCs were able to proliferate and migrate on both EFS1 and BIIEFS (Fig. 4(a)). EFS1 and BIIEFS showed similar cell live-dead ratios to the control group (Fig. 4 (b)). The morphology of the BMSCs seeded on electrospun fibers scaffolds was examined using cytoskeletal and nuclear staining (Fig. 4(c)). Compared to the control group, BMSCs on EFS1 and BIIEFS showed more pseudopodia-like protrusions, indicating that the cells were able to adhere well to the EFS1 and BIIEFS.

We then measured the cell viability using CCK-8 assays (Fig. 4(d)). At one and three days, there were no significant differences between the absorbance indices of all the samples. At five days, the absorbance index of BIIEFS (1.24 ± 0.05) was considerably greater than that of EFS1 (0.89 ± 0.17), which might be a result of strontium's ability to stimulate the proliferation of BMSCs [32]. In addition, the progressively increasing absorbance index suggested that BMSCs could proliferate efficiently on EFS1 and BIIEFS. Collectively, these results demonstrated that BIIEFS were suitable for the migration and proliferation of BMSCs.

3.4. Bi-lineage inducible effects of BIIEFS in vitro

The osteogenic and chondrogenic capacities of BMSCs were evaluated to determine whether BIIEFS could promote the bi-lineage differentiation of stem cells. ARS staining (red) at 21 days and ALP staining (violet) at 7 days demonstrated that the BIIEFS extract increased cellular mineralization and ALP activity (Fig. 5(a)). After ARS staining, cetylpyridinium chloride solutions were used to dissolve the calcium deposits. The results indicated that BMSCs cultured with BIIEFS extract had greater calcium deposition, as evidenced by the absorbance index at 565 nm (1.99 ± 0.13) (Fig. 5(b)). The ALP activity results were consistent with the ARS staining, as shown in Fig. 5(c). The capacity of electrospun fibers scaffolds to promote osteogenesis in BMSCs was evaluated by the measurement of osteogenesis markers using immunofluorescence staining, RT-qPCR, and western blotting. After 14 days of osteogenic induction with the electrospun fibers scaffold extract, higher levels of green fluorescence were observed in the cytoplasm, suggesting that BIIEFS facilitated the expression of collagen I and osteocalcin (as shown in Fig. 5(d) and Fig. S6(a)). The intensity of immunofluorescence of Runx2, a transcription factor located in the nucleus, was increased after induction with the BIIEFS extract medium, as shown in Fig. 5(d). The results of the semiquantitative analysis demonstrated that the extract of BIIEFS increased, the expression of collagen I (37.58 ± 2.20 A U.), osteocalcin (39.98 ± 1.64 A U.), and Runx2 (47.22 ± 2.06 A U.), shown by the mean immunofluorescence intensity (Figs. S6(b) and S6 (c), S6(d)). Fold changes indicating expression of *Col1a1*, *OCN*, and *Runx2* were significantly increased after exposure to the BIIEFS extract (6.94 ± 0.31, 3.01 ± 0.49, and 2.09 ± 0.45, respectively), compared with EFS1 (1.02 ± 0.10, 1.01 ± 0.07, and 0.95 ± 0.06, respectively), and the control (0.97 ± 0.04, 0.98 ± 0.09, and 0.95 ± 0.11, respectively), as illustrated in Fig. 5(e), (f), and 5(g). The protein expression levels of collagen I, osteocalcin, and Runx2 were evaluated by western blotting, as shown in Fig. 5(h). It was found that the BIIEFS extract facilitated the protein expression of collagen I, osteocalcin, and Runx2 in comparison with EFS1 and the control. This was demonstrated through semiquantitative analysis of the relative gray values of the bands, which yielded values of 1.01 ± 0.23, 1.11 ± 0.09, and 1.10 ± 0.09 for the expression of collagen I, osteocalcin, and Runx, respectively, after culture in BIIEFS extract, 0.42 ± 0.03, 0.46 ± 0.15, and 0.49 ± 0.16,

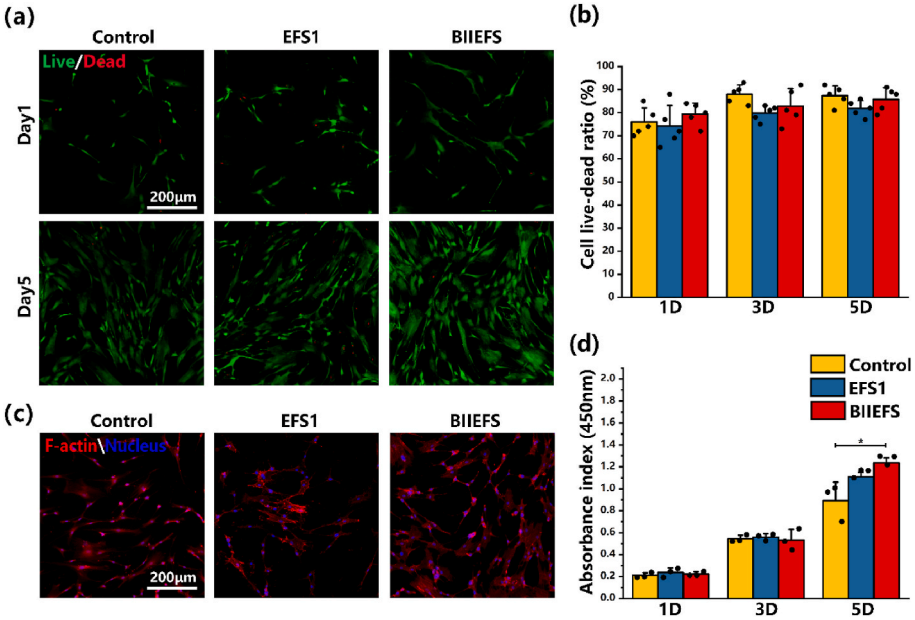

Fig. 4. Biocompatibility of electrospun fibers scaffolds. (a) Fluorescence images of living and dead BMSCs seeded on empty wells, EFS1, and BIIEFS. (b) The cell live-dead ratio of BMSCs seeded on empty wells, EFS1, and BIIEFS at 1, 3, and 5 days. (c) Cytoskeletal staining of BMSCs seeded on empty wells, EFS1, and BIIEFS at 3 days. (d) The absorbance indices of BMSCs seeded on empty wells, EFS1, and BIIEFS at 1, 3, and 5 days. (*$p < 0.05$).

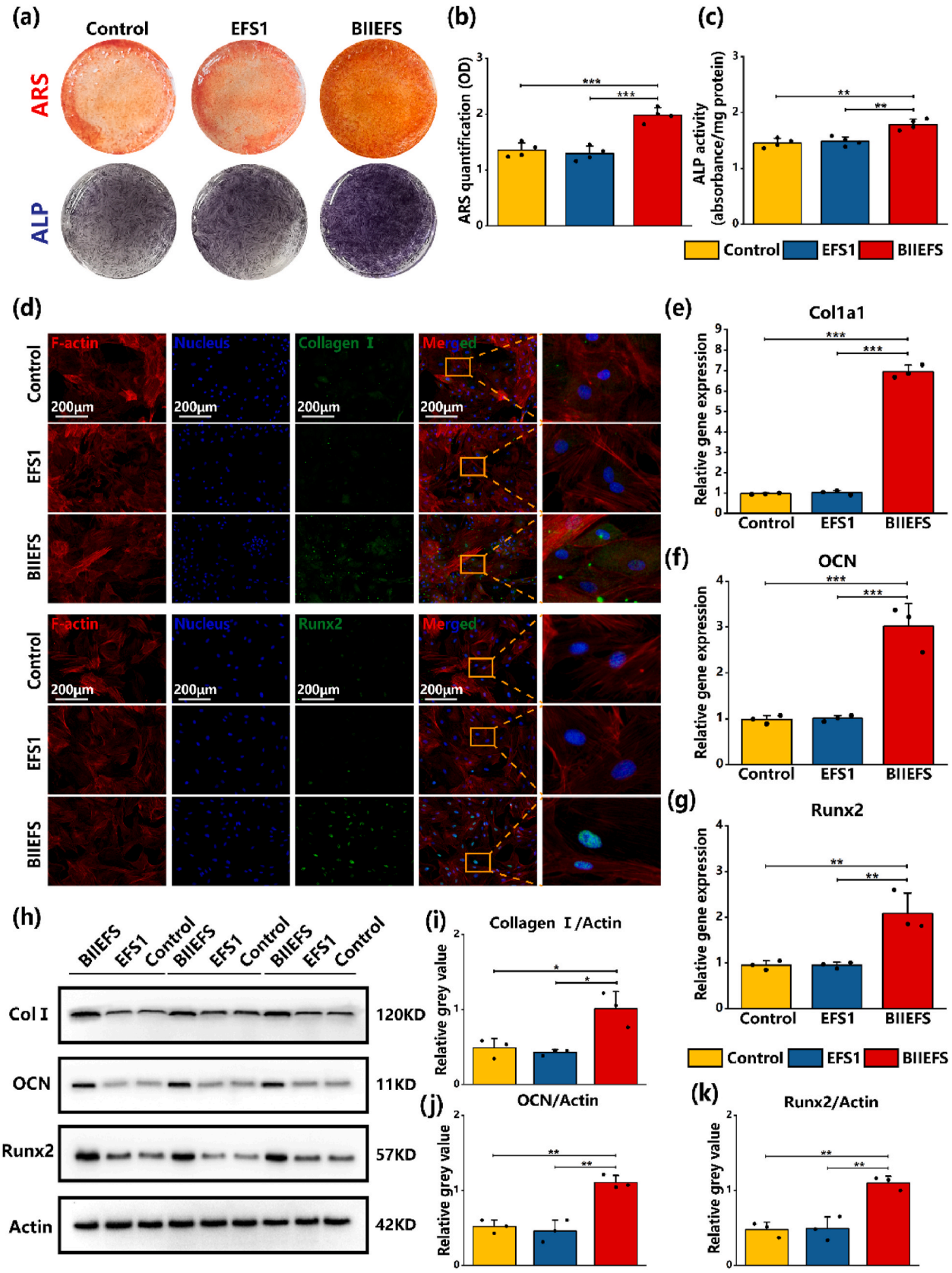

Fig. 5. Effect of electrospun fibers scaffolds on osteogenesis *in vitro*. (a) ARS staining at 21 days and ALP staining at 7 days. (b) Qquantification of cellular mineralization. (c) ALP activity at 7 days. (d) Immunofluorescence staining of collagen I and Runx2 in BMSCs after 14 days of osteogenic induction with extracts of electrospun fibers scaffolds. (e)–(g) RT-qPCR measurement of *Col1a1*, *Ocn*, and *Runx2* gene expression BMSCs after 14 days of osteogenic induction with extracts of electrospun fibers scaffolds. (h) Western blotting showing expression of collagen I, Ocn, Runx2, and actin. (i)–(k) Semiquantitative protein expression of collagen I, OCN, and Runx2. (*$p < 0.05$, **$p < 0.01$, and ***$p < 0.001$).

respectively, after culture with EFS1, and 0.48 ± 0.13, 0.52 ± 0.09, and 0.48 ± 0.10, respectively, in the control, as shown in Fig. 5(i), (j), and 5 (k). The western blotting and semiquantitative measurement results were thus consistent with the immunofluorescence and RT-qPCR results. These findings verified that the BIIEFS extract significantly enhanced osteogenesis in an *in vitro* setting.

Additionally, the extract was used to evaluate the chondrogenic potential of electrospun fibers scaffolds in BMSCs. The gross appearance of the cartilage pellets was a milky white color with an irregular spherical shape (Fig. S7(a)). Alcian Blue and Safranin-O staining of the pellet cultured with BIIEFS extract induction medium showed highest dyeing depth, which demonstrated increased proteoglycan and extracellular matrix synthesis in pellets cultured in BIIEFS extract induction medium (Fig. 6(a), S7(b)). The strongest intensity of collagen II IHC staining in the cartilage pellets revealed that the BIIEFS extract medium was more effective in stimulating collagen II synthesis and secretion compared to EFS1 and the control, as shown in Fig. 6(a). The findings indicate that the cartilage pellets cultured with BIIEFS extract medium were larger in volume (3.01 ± 0.45 mm^3) compared to those cultured with EFS1 (1.73 ± 0.25 mm^3) and the control group (1.67 ± 0.19 mm^3), as illustrated in Fig. 6(b). In terms of the Bern histological score, it was observed that cartilage pellets cultured with BIIEFS extract showed the highest scores (6.00 ± 0.81) compared with those in the other two groups (Fig. 6(c)). Immunofluorescence staining indicated marked increases in the collagen II and aggrecan contents in the cytoplasm, as well as the content of Sox9 in the nucleus, following a 21-day chondrogenic induction with the BIIEFS extract induction medium (as illustrated in Fig. 6(d) and S7(c)). Semiquantitative analysis of the mean immunofluorescence intensity also revealed that the BIIEFS extract had a positive effect on the expression of collagen II (50.87 ± 2.53 A U.), aggrecan (41.19 ± 2.62 A U.), and Sox9 (77.13 ± 7.60 A U.) as shown in Figs. S7 (d) and S7(e), and S7(f). The BIIEFS extract also had a significant effect on the expression of the chondrogenic marker genes *Col2a1*, *Aggrecan*, and *Sox9*, as demonstrated by RT-qPCR. The expression levels of these genes were found to be higher in the BIIEFS extract induction medium (2.20 ± 0.30, 2.23 ± 0.44, and 1.68 ± 0.21, respectively) compared to the EFS1 extract induction medium (1.13 ± 0.07, 1.0 ± 0.10, and 1.03 ± 0.11, respectively) and the control (0.97 ± 0.13, 1.06 ± 0.09, and 0.97 ± 0.10, respectively), as shown in Fig. 6(e), (f), and 6(g). The protein levels of collagen II, aggrecan, and Sox9 were analyzed using western blotting. The findings were consistent with those of immunofluorescent staining and RT-qPCR, as depicted in Fig. 6(h). The BIIEFS extract induction medium promoted the protein expression of collagen II, aggrecan, and Sox9 compared to the EFS1 and control groups, as shown by the semiquantitative analysis of the gray values of the bands, with values of 1.15 ± 0.14, 0.83 ± 0.18, and 0.96 ± 0.17 for collagen II, aggrecan, and Sox9, respectively, in BIIEFS extract, 0.24 ± 0.05, 0.33 ± 0.08, and 0.24 ± 0.03, respectively, for EFS1, and 0.27 ± 0.03, 0.36 ± 0.13, and 0.27 ± 0.08, respectively, for the control (Fig. 6(i), (j), 6(k)). These results suggested that BIIEFS promoted BMSC chondrogenesis and osteogenesis *in vitro*.

We further investigated the impact of BIIEFS on tenogenic differentiation of TDSCs. The expression levels of relevant tenogenic marker genes and proteins of TDSCs were measured after culturing in DMEM, EFS1 extract medium, and BIIEFS extract medium for 72 h. Immunofluorescence showed that the BIIEFS and EFS1 extract media did not promote the expression of tenomodulin (Tnmd) and scleraxis (Scx) proteins (Figs. S8(a) and S8(b), S8(c), S8(d)), while RT-qPCR results indicated that neither EFS1 nor BIIEFS extract media significantly increased the mRNA levels of tenogenic marker genes (Figs. S8(e) and S8 (f), S8(g)). We next conducted Sirius Red staining to evaluate collagen deposition in TDSCs, which showed that collagen deposition in TDSCs cultured with the BIIEFS extract was similar to EFS1 and control groups (Fig. S9(a)). Western blotting and quantitation of the band also demonstrated that BIIEFS extract medium failed to promote the expression of Tnmd and Scx (Figs. S9(b) and S(c), S(d)). These results indicated that BIIEFS was unable to promote tenogenic differentiation of TDSCs *in vitro*.

3.5. Immunoregulatory effect of BIIEFS in vitro

Previous research has indicated that scaffolds incorporating strontium and other bioactive ions are able to modulate macrophage polarization and also show immunoregulatory properties [23]. RAW 264.7 cells were used to examine the ability of BIIEFS to modulate macrophage polarization. RAW 264.7 cells were cultured in media containing BIIEFS extract, EFS1 extract, and DMEM only. The media were supplemented with LPS to simulate acute inflammation following the rotator cuff tear, while IL-4 and IL-13 were added to the cultures to simulate the resolution of inflammation after acute injury. The results of the immunofluorescent staining of the M1 macrophage marker inducible nitric-oxide synthase (iNOS) and the M2 macrophage marker Arginase-1 (Arg-1) indicated that culture with the BIIEFS extract medium resulted in reduced iNOS expression following LPS stimulation. Additionally, the BIIEFS extract medium induced increased expression of *Arg-1* in the presence of IL-4 and IL-13, as shown in Fig. 7(a) and (b). Flow cytometry was used to determine the proportions of M1 and M2 macrophages after culture in the different media. The results indicated that culture with the BIIEFS extract medium significantly reduced the percentage of iNOS-positive M1 macrophages (52.27 ± 2.22%), compared to the EFS1 extract medium (65.17 ± 1.31%) and DMEM only (67.13 ± 1.16%) (as shown in Fig. 7(c) and (d)). Furthermore, it was observed that the percentage of CD206-positive M2 macrophages was increased after cultured with BIIEFS extract medium (50.17 ± 1.72%) as illustrated in Fig. 7(e) and (f). The fold changes of expression of the M1 macrophage marker genes *IL-1β*, *CD80*, and *TNF-α* were significantly reduced when exposed to the BIIEFS extract medium (0.47 ± 0.04, 0.22 ± 0.03, and 0.47 ± 0.04, respectively) compared to the EFS1 extract medium (1.03 ± 0.08, 1.00 ± 0.10, and 1.12 ± 0.13, respectively) and DMEM only (1.00 ± 0.11, 1.00 ± 0.10, and 1.00 ± 0.04, respectively), as shown in Fig. 7(g). The fold changes of expression of the M2 macrophage marker genes *IL10*, *CD206*, and *Arg-1* were observed to be significantly higher in the presence of the BIIEFS extract medium (2.76 ± 0.30, 6.99 ± 0.48, and 3.67 ± 0.65, respectively) as compared to the EFS1 extract medium (1.24 ± 0.04, 1.07 ± 0.04, and 0.93 ± 0.09, respectively) and DMEM only (1.07 ± 0.11, 1.01 ± 0.06, and 1.02 ± 0.08, respectively), as shown in Fig. 7(h). These findings indicated that BIIEFS could modulate macrophage polarization and mitigate the negative effects of acute inflammation.

3.6. Effect of BIIEFS on tendon-to-bone interface synchronous regeneration in vivo

According to reports, the regeneration of fibrocartilage layers at the tendon-to-bone interface is unsuccessful following rotator cuff tears, and bone loss occurs in the greater tuberosity of the humerus [10]. Therefore, the most important aspect of tendon-bone healing involves strategies to promote regeneration of the fibrocartilage layer while enhancing bone regeneration at the greater tuberosity. Tenocytes and fibrochondrocytes show an orderly arrangement at the native tendon-to-bone interface (Fig. S10(a)). The tendon is connected to the bone through two fibrocartilage layers, which are separated by a tidemark (Fig. S10(a)). The extracellular matrix of tendon and bone is composed primarily of type I collagen, whereas the extracellular matrix of two fibrocartilage layers is primarily composed of type II collagen. Histological, micro-CT, biomechanical, and IHC analyses were conducted at 4 and 8 weeks following the surgical procedure to assess the regeneration and inflammation status of the tendon-to-bone interface, as illustrated in Fig. S10(b).

The BMD and BV/TV of the greater tuberosity were evaluated using micro CT. From the cross-sectional view at the maximum diameter of the humeral head, it was evident that bone loss occurred predominantly in

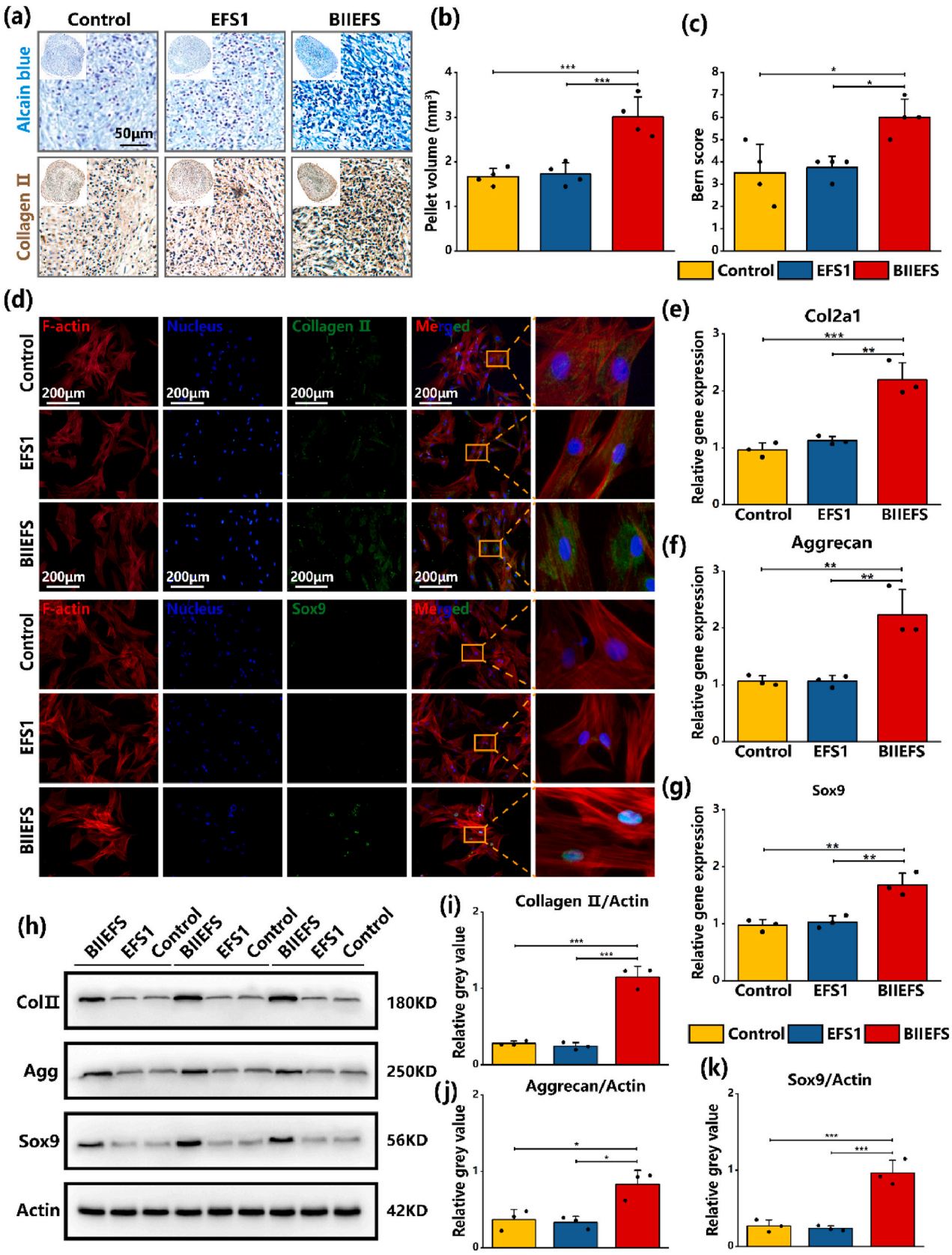

Fig. 6. Effect of electrospun fibers scaffolds on chondrogenesis *in vitro*. (a) Alcain Blue and collagen II IHC staining of pellets. (b) Volumes of pellets cultured with different extract induction media. (c) Bern scores for cartilage pellets. (d) Immunofluorescent staining of collagen II and Sox9 in BMSCs after 21 days of chondrogenic induction with extracts of electrospun fibers scaffolds. (e)–(g) RT-qPCR measurement of the expression of *Col2a1*, *Aggrecan*, and *Sox9* in BMSCs after 21 days of chondrogenic induction with extracts of electrospun fibers scaffolds. (h) Western blotting showing expression of collagen II, aggrecan, and Sox9 proteins. (i)–(k) Semiquantitative protein expression levels of collagen II, aggrecan, and Sox9. (*$p < 0.05$, **$p < 0.01$, and ***$p < 0.001$).

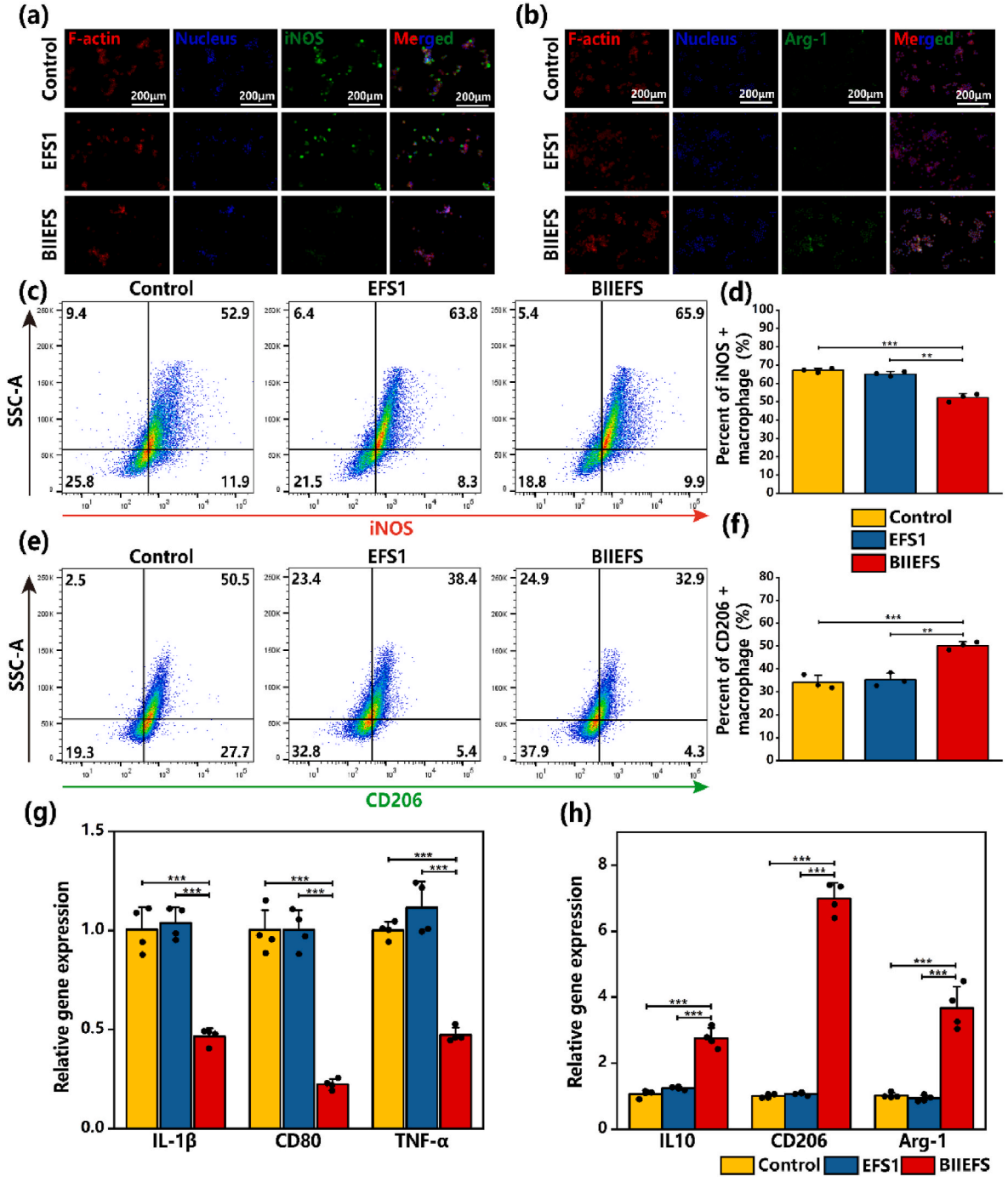

Fig. 7. Immunoregulatory effect of electrospun fibers scaffolds. (a) Immunofluorescence staining of iNOS in RAW 264.7 cells after LPS stimulation. (b) Immunofluorescence staining of Arg-1 in RAW 264.7 cells following incubation with IL-4 and IL-13. (c)–(d) Flow cytometry of iNOS-positive M1 macrophages. (e)–(f) Flow cytometry of the CD206-positive M2 macrophages. (g) RT-qPCR measurement of changes in the expression of *IL-1β*, *CD80*, and *TNF-α* in M1 macrophages. (h) RT-qPCR measurement of changes in the expression of *IL10*, *CD206*, and *Arg-1* in M2 macrophages. (**p < 0.01, and ***p < 0.001).

the greater tuberosity of the humerus in the defect group, and that bone regeneration was minimal in the simple-repair and EFS1 groups at four weeks. In addition, compared to the other three groups, BIIEFS substantially promoted bone regeneration of the greater tuberosity at four and eight weeks (Fig. 8(a)). The examination of BMD indicated that BIIEFS enhanced bone density (0.63 ± 0.05 g/cm^3), compared to the remaining groups (Fig. 8(b)). It was found that BIIEFS led to a significant increase in BV/TV after four weeks (58.36 ± 8.54%) but there was no significant difference in the BV/TV between the BIIEFS group (64.58 ± 3.85%) and the EFS1 group (54.35 ± 5.47%) after eight weeks, as shown in Fig. 8(c). According to these findings, BIIEFS promoted bone regeneration at the tendon-to-bone interface.

At four weeks, HE and Safranin O/Fast Green staining showed that the fibrocartilage in the defect group had not regenerated (Fig. 8(d) and (e)). However, a four weeks, fibrocartilage regeneration was markedly greater in the BIIEFS group compared to both the simple-repair and the EFS1 groups (Fig. 8(d) and (e)). At eight weeks, little regenerative fibrocartilage was observed in the defect, simple-repair, and EFS1 groups (Fig. 8(d) and (e)). In contrast, more regenerative fibrocartilage was observed in the BIIEFS group, indicating that BIIEFS promoted

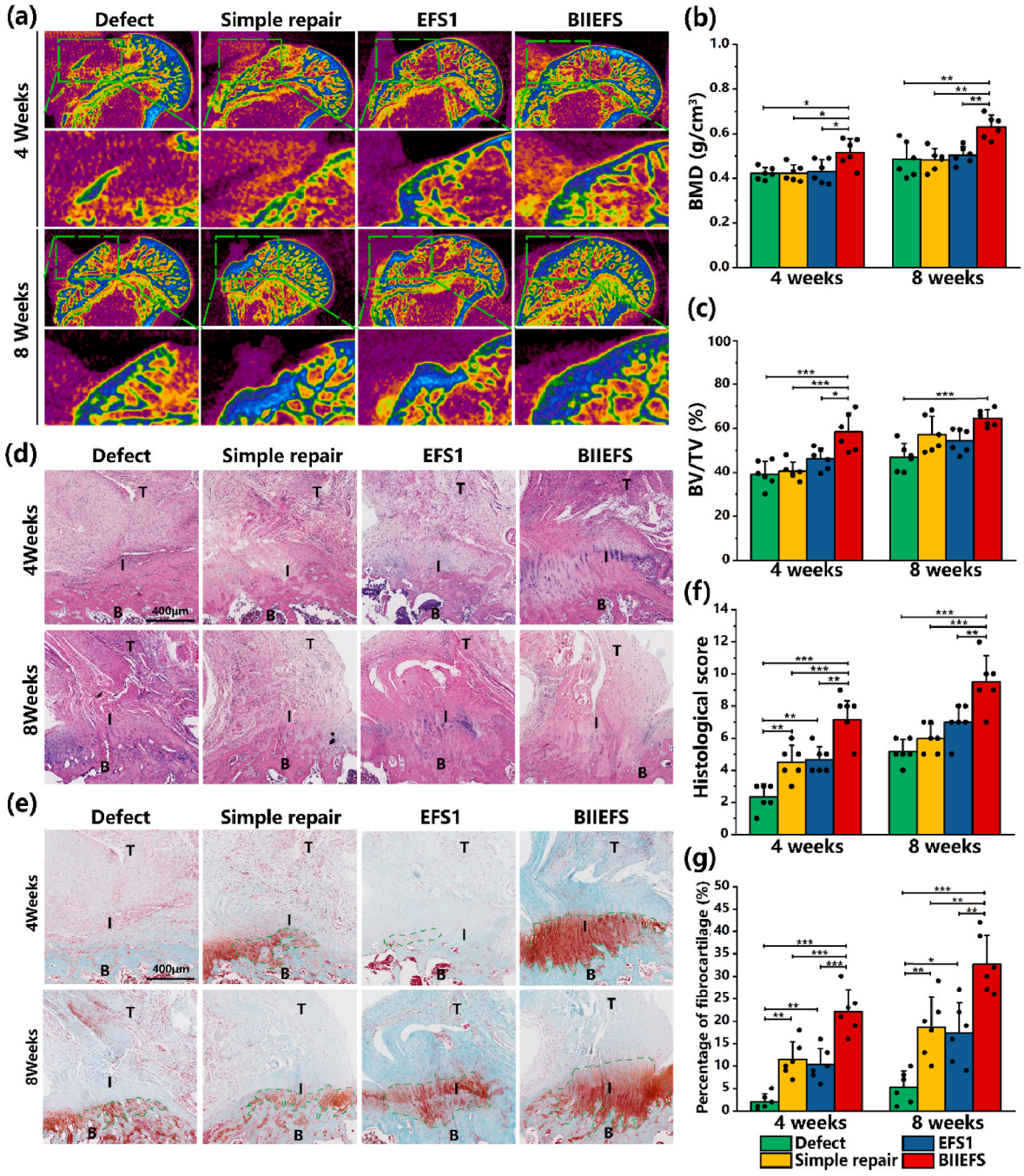

Fig. 8. Micro-CT and histological analyses *in vivo*. (a) Micro-CT images of the cross-sectional view of the humeral head at four and eight weeks. (b)–(c) BMD and BV/TV values of the tendon-to-bone interface. (d)–(e) HE and Safranin O/Fast Green staining of the tendon-to-bone interface. (f) Histological scores of the defect, simple-repair, EFS1, and BIIEFS groups. (g) Percentages of fibrocartilage in the defect, simple-repair, EFS1, and BIIEFS groups. T: tendon, I: tendon-to-bone interface, B: bone. The area circled by the green dashed line represents the fibrocartilage. (*$p < 0.05$, **$p < 0.01$, and ***$p < 0.001$).

regeneration of the tendon-to-bone interface fibrocartilage layer (Fig. 8 (d) and (e)). Unfortunately, there was no restoration of the tidemark in any of the groups. At eight weeks, it was observed that the BIIEFS group had the highest histological score (9.50 ± 1.64) and percentage of fibrocartilage (32.67 ± 6.50%) in comparison to the other three groups. This suggests that BIIEFS was successful in promoting the regeneration of the tendon-to-bone interface, as depicted in Fig. 8(f). Toluidine blue staining indicated that, at eight weeks, the metachromatic area of the BIIEFS group (3.35 ± 0.60 × 10^5 μm^2) was larger than that of the simple-repair (1.48 ± 0.43 × 105 μm2) and EFS1 group (2.03 ± 0.57 × 10^5 μm^2), as shown in Figs. S11(a) and S11(b). We further evaluated the tendon-maturing score to assess tendon regeneration *in vivo*. We found that BIIEFS (9.83 ± 0.98) had higer tendon-maturing score compared to defect group (8.00 ± 0.63) and simple repair group (8.50 ± 0.55) at eight weeks (Fig. S12(a)).

Fibrocartilage layer regeneration and inflammation were evaluated by IHC at the tendon-to-bone interface. In contrast to the other three groups, a larger positive area and enhanced staining intensity of collagen II were observed in the BIIEFS group, indicating that BIIEFS facilitated fibrocartilage layer regeneration in situ (Fig. 9(a)). At four and eight weeks, CD206 IHC staining revealed that the BIIEFS group contained more CD206-positive M2 macrophages than the defect, simple-repair, and EFS1 groups (Fig. 9(b). The BIIEFS group also showed greater numbers of CD206-positive M2 macrophages at the tendon-to-

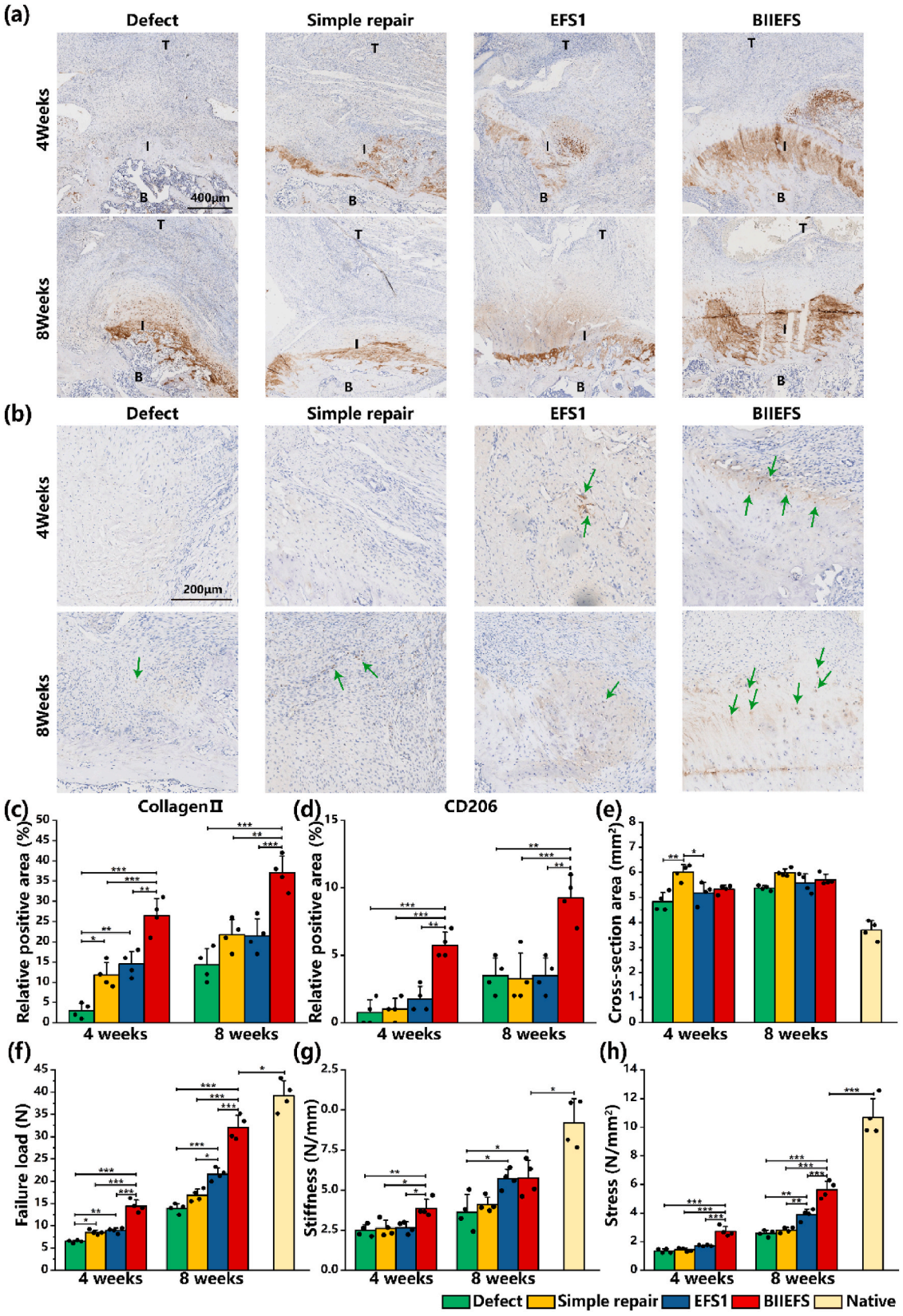

Fig. 9. Immunohistochemical staining and mechanical properties of the tendon-to-bone interface. (a) Immunohistochemical staining of collagen II at the tendon-to-bone interface. (b) Immunohistochemical staining of CD206 at the tendon-to-bone interface. Green arrow: CD206-positive macrophages. (c) Relative positive area of collagen II. (d) Relative positive area of CD206. (e)–(h) Cross-sectional area, failure load, stiffness, and stress of the tendon-to-bone interface. T: tendon, I: tendon-to-bone interface, B: bone. (*$p < 0.05$, **$p < 0.01$, and ***$p < 0.001$).

bone interface in comparison to the other three groups, as depicted in Fig. 9(b). The findings indicate that BIIEFS significantly improved the regeneration of the fibrocartilage layer during tendon-bone healing, as shown by the increased area of collagen II positivity at the tendon-to-bone interface (37.00 ± 4.16%) (Fig. 9(c)). The BIIEFS group (9.25.00 ± 1.71%) showed the greatest area of CD206 positivity. This suggested that BIIEFS can accelerate the polarization of anti-inflammatory M2 macrophages, which is believed to have a positive impact on tissue regeneration (Fig. 9(d)). These results suggested that BIIEFS could not only promote fibrocartilage layer regeneration directly but also accelerate tissue regeneration by modulating macrophage polarization.

As previously reported, the biomechanical properties were measured to assess the regenerative effect *in vivo* [33]. At four and eight weeks, there was a modest difference in the cross-sectional area between the simple-repair group and the defect group (Fig. 9(e)). The BIIEFS group exhibited a significantly higher failure load (14.40 ± 1.36 N) compared to the defect group (6.48 ± 0.29 N), simple-repair group (8.53 ± 0.51 N), and EFS1 group (8.93 ± 0.56 N) after four weeks, as illustrated in Fig. 9(f). At eight weeks, it was observed that the BIIEFS group exhibited a significantly higher failure load (32.08 ± 2.71 N) in comparison to the other three groups (Fig. 9(f)). However, there was still a gap between the failure load of the repaired rotator cuff using BIIEFS and that of the native rotator cuff (39.18 ± 3.41 N) (Fig. 9(f)). After four weeks, it was observed that the BIIEFS group exhibited greater stiffness (5.75 ± 1.10 N/mm) in comparison to the remaining three groups, as shown in Fig. 9 (g). At eight weeks, however, there was no statistically significant difference in stiffness between the BIIEFS group (5.75 ± 1.10 N/mm) and the EFS1 group (5.70 ± 0.60 N/mm). The stress levels of the BIIEFS group were observed to be significantly higher than the other three groups at four and eight weeks, as indicated by the values of 2.71 ± 0.34 N/mm^2 and 5.63 ± 0.58 N/mm^2, respectively (Fig. 9(h)). The outcomes of the biomechanical tests indicated that BIIEFS could facilitate the recovery of rotator cuff function. Therefore, we consider that BIIEFS could restore the function of the tendon-to-bone interface by promoting its regeneration.

4. Discussion

In this study, we fabricated novel electrospun fibers scaffolds containing Sr-MBG. The electrospun fibers scaffolds were capable of sustained release of various bioactive ions, thereby catering to the requirements of synchronous regeneration of the tendon-to-bone interface. Moreover, these novel electrospun fibers scaffolds had immunoregulatory properties, promoting the polarization of macrophages towards a favorable phenotype for tendon-to-bone interface regeneration. Our research highlighted the significance of the synchronous regeneration of soft and hard tissues at the tendon-to-bone interface, as well as the great application potential of bioactive element-doped mesoporous bioactive glass nanoparticles on soft-to-hard interface regeneration.

The high incidence of retear after rotator cuff repair is one of the challengeable issues in clinical practice. Age, inferior tendon quality, larger tear size, lower bone mineral density, and diabetes mellitus are risk factors for retear [34,35]. Retear can be classified into two types. Retear at the tendon-to-bone interface is type 1 retear and retear at the medial rotator cuff is type 2 retear [36]. Some clinical researches have compared the postoperative retear pattern of different rotator cuff repair procedures and found that the retear pattern varies considerably between specific surgical procedures. Cummins et al. observed 22 patients with retear after rotator cuff repair using suture anchors and a mattress-suturing configuration. Nineteen of the retears were tendon pulling through sutures, which could be seen as type 2 retear [37]. Cho et al. compared the effects of single-row technique and suture bridge on retear patterns [38]. They found that 73.7% retears in single-row group were type 1 retear, while only 25.9% retears in suture bridge group were type 1 retear [38]. Hayashida et al. evaluated postoperative retear patterns in 47 patients undergoing double-row rotator cuff repair [39]. There were 13 cases of retear, while 4 of them were complete retearing of the tendon from the footprint, which was type 1 retear [39]. The above studies suggested that although the retear patterns of distinct surgical procedures were significantly different, there was still a considerable proportion of patients experiencing retears at the tendon-to-bone interface. Currently, it is believed that type 1 retear is associated with inadequate tendon-to-bone interface regeneration, whereas type 2 retear is associated with degeneration of the tendon that results in poor tendon quality [36,40]. Therefore, promoting tendon-to-bone interface regeneration may be the optimal method to reduce the chance of type 1 retear.

The tendon-to-bone interface is a unique connection between tendons and bones. The tensile modulus of the tendon is approximately 0.45 GPa, while that of the bone is approximately 20 Gpa [41]. On the interface between mechanically mismatched soft and hard materials, stress concentration induced by stress shielding significantly increases the chance of failure [4,41]. The heterogeneous structure of the tendon-to-bone interface reduces the stress concentration induced by the mismatched mechanical properties of the tendon and bone, enabling the tendon-to-bone interface to withstand greater external forces [2]. Moffat et al. reported that the function of the tendon-to-bone interface is directly related to the fibrocartilage layer within the interface [42]. The fibrocartilage layer at the tendon-to-bone interface possesses mechanical properties that bridge the gap between the tendon and bone, thereby reducing the stress concentration resulting from the mismatch in mechanical properties between the different tissues [42]. Schwartz et al. observed that a loss of mineralized fibrocartilage during development significantly reduced the biomechanical function of the tendon-to-bone interface [43]. These findings highlight the crucial importance of the fibrocartilage layer in the functioning of the tendon-to-bone interface. Unfortunately, fibrocartilage is unable to regenerate and is thus replaced by scar tissue even with surgical repair, resulting in a significantly increased chance of retear [44,45]. In addition, bone loss occurs in the surrounding bone after tendon-to-bone interface injury due to the reduced loading and increased activity of osteoclasts, which is detrimental to tendon-bone healing [11,46]. Therefore, the optimal biomaterials for tendon-bone healing would encourage the synchronous regeneration of fibrocartilage and bone.

The inflammatory response following injury is not favorable to the regeneration of the fibrocartilage and is the cause of surrounding bone loss [13,15]. During the acute inflammatory phase in the tendon-bone healing process, a large number of macrophages are recruited to the tendon-to-bone interface. These macrophages are polarized to the M1 pro-inflammatory phenotype that secretes large amounts of pro-inflammatory cytokines [14,47]. The pro-inflammatory factors inhibit osteogenic and chondrogenic differentiation of mesenchymal stem cells, impeding the regeneration of fibrocartilage and bone tissue at the tendon-to-bone interface [48,49]. Furthermore, these pro-inflammatory factors also promote the formation of osteoclasts and enhance their activity, accelerating the loss of surrounding bone at the tendon-to-bone interface [50,51]. In contrast to M1 macrophages, anti-inflammatory M2 macrophages can promote tissue regeneration and resolve inflammation by secreting factors such as IL-4 and IL-10 [15, 52]. Unfortunately, there are insufficient numbers of M2 macrophages during the tendon-bone healing process, resulting in a chronic and dysregulated inflammatory response that is unfavorable for tendon-to-bone interface regeneration. Previous studies have indicated that mesenchymal stem cell-derived exosomes were able to regulate M1/M2 macrophage polarization during tendon-bone healing to accelerate the regeneration of the tendon-bone interface [53,54]. Li et al. discovered that accelerating the polarization of M2 macrophages through chondroitin sulfate enhanced the effect of BMP-2 in promoting bone regeneration at the tendon-to-bone interface [55]. Therefore, immunoregulatory biomaterials that facilitate the polarization of M2 macrophages are able to accelerate tendon-bone healing.

MBGs possess remarkable osteogenic and angiogenic properties. They also have anti-inflammatory, antibacterial, and anticancer properties when incorporating bioactive elements such as Li, Zn, and Ce, which enables the MBG to satisfy the diverse tissue regeneration requirements [18,56,57]. Fan et al. constructed a microgel bone powder based on cerium (Ce) and selenium (Se) elements co-doped with mesoporous bioactive glass, sodium alginate (SA), and collagen [58]. These Ce and Se co-doped mesoporous bioactive glass were able to suppress osteoma cell growth and stimulate new bone formation [58]. Kurtuldu et al. prepared cerium-containing mesoporous bioactive glass nanoparticles that inhibited the release of nitric oxide from macrophages stimulated with LPS, demonstrating their outstanding antibacterial properties [59]. Strontium is a trace element present in the human skeletal system [60]. Doping strontium to bioactive glass can further enhance its osteogenic and angiogenic properties [21,61]. Interestingly, it has been discovered that strontium ions and strontium-containing bioactive glass promote the chondrogenesis of mesenchymal stem cells and facilitate the polarization of macrophages towards the favorable M2 phenotype [62–64]. Therefore, doping bioactive elements enhances the bioactivity of mesoporous bioactive glass, endowing it with versatile functions, and indicating its potential for the regeneration of soft and hard tissue.

Our research revealed that BIIEFS can stimulate the polarization of M2 macrophages *in vivo* and induce the synchronous regeneration of the tendon-to-bone interface. Dong et al. discovered that the extract of bioactive glass promoted polarization of RAW 264.7 macrophages to the M2 phenotype, which was associated with the release of silicon ions from the bioactive glass [65]. Zhao et al. discovered that strontium-containing bioactive glass microspheres (SrBGM) promoted the polarization of RAW 264.7 macrophages toward the M2 phenotype [22]. This study found that bioactive glass microspheres (BGM) without strontium and strontium chloride ($SrCl_2$) promoted polarization of M2 macrophages and also reduced the transcription levels of pro-inflammatory factors [22]. Surprisingly, SrBGM exhibited the best immunoregulatory abilities compared to BGM and $SrCl_2$, which indicated that the incorporation of strontium enhanced the immunoregulatory properties of bioactive glass [22]. Therefore, we speculated that the immunomodulatory effect of BIIEFS was derived from the release of silicon and strontium ions during the degradation process. These bioactive ions stimulated the polarization of macrophages towards favorable M2 phenotype at the tendon-to-bone interface.

The degradation of BIIEFS resulted in an ionic microenvironment containing strontium, silicon, and calcium ions in the surrounding area. Calcium, strontium, and silicon ions are able to stimulate the expression of pro-osteogenic markers such as Runx2 and OCN, thereby promoting bone tissue regeneration [66,67]. Moreover, both strontium and silicon can reduce bone resorption by inhibiting RANKL-mediated osteoclast activation [66,67]. On the basis of previous studies, we hypothesized bioactive ions released from BIIEFS inhibited osteoclast activity and promoted osteogenic differentiation of osteoblasts, improving bone regeneration at the tendon-to-bone interface. Previous studies have reported that strontium can enhance chondrogenesis of MSCs and accelerate articular cartilage regeneration by promoting M2 polarization of macrophages [23,68,69]. Therefore, we hypothesized that the strontium ions released by BIIEFS can enhance chondrogenic differentiation of MSCs at the tendon-to-bone interface and accelerate fibrocartilage regeneration by modulating the appropriate macrophage phenotype. Although BIIEFS could not promote tenogenesis of TDSC *in vitro*, we found that BIIEFS could increase tendon-maturing socre of tendon. Previous studies reported that M2 macrophages were able to accelerate tendon regeneration [70–72]. So we thought that BIIEFS facilitated tendon regeneration through immunoregulatory effect. We believe that BIIEFS create an ionic microenvironment at the tendon-to-bone interface during the degradation process. Diverse bioactive ions in this microenvironment can exert bi-lineage inducible and immunomodulatory effects to specific cells, thereby fostering the synchronous regeneration of tendon-to-bone interface.

There are several limitations to this study. Firstly, the quantification of various ions in the blood and their associated adverse effects was not conducted. Secondly, the animal model utilized in this study was acute rotator cuff injury in rats. The regenerative abilities of rats are superior to those of humans. Additionally, the predominant type of rotator cuff tear observed in clinical settings is chronic. Consequently, conducting additional examinations and verification in a chronic rotator cuff tear model of large animals could enhance the credibility of BIIEFS in stimulating tendon-bone healing. Thirdly, we found that the extract of BIIEFS was unable to improve tenogenesis of TDSCs *in vitro*. Previous studies have reported that molybdenum (Mo) and zinc (Zn) ions can promote tenogenic differentiation of TDSCs [29,73]. By incorporating Mo or Zn ions into mesoporous bioactive glass in future research, it may be feasible to improve the capacity of electrospun fibers scaffolds to promote tendon regeneration. Fourthly, our research mainly focused on the effect of tendon-to-bone interface regeneration on rotator cuff. However, not all retears occur at the tendon-to-bone interface, and the causes of rotator cuff retears have not been fully elucidated. Therefore, more in-depth research on the mechanism of retear is needed in the future to develop more effective threapy to reduce the incidence of retear.

5. Conclusion

In conclusion, this study described the successful development of electrospun fibers scaffolds that possessed immunomodulatory capabilities and effectively enhanced regeneration of the tendon-to-bone interface. BIIEFS containing strontium-doped mesoporous bioactive glass nanoparticles were found to continuously release multiple bioactive ions. BIIEFS demonstrated excellent biocompatibility and promoted the differentiation of mesenchymal stem cells to both osteogenic and chondrogenic lineages. Furthermore, BIIEFS exhibited immunomodulatory properties and could promote the polarization of RAW 264.7 macrophages to the M2 phenotype *in vitro*. After implantation in the injured tendon-to-bone interface, BIIEFS was able to promote macrophage polarization to the favorable M2 phenotype and stimulate the synchronous regeneration of the tendon-to-bone interface, thereby restoring the biomechanical strength of the rotator cuff. Our study provided a novel perspective on the use of electrospun scaffolds incorporating mesoporous bioglass nanoparticles for the in situ regeneration of heterogeneous interface tissue through versatile bioactive ions.

Authors' contributions

Haihan Gao contributed to conceptualization, methodology, investigation, date curation, and writing the original article. Liren Wang contributed to methodology, investigation, validation, and writing the original article. Zhiqi Lin contributed to investigation and formal analysis. Haocheng Jin contributed to visualization and formal analysis. Yangbao Lyu contributed to investigation. Yuhao Kang contributed to methodology. Tonghe Zhu reviewed and edited the article. Jinzhong Zhao contributed to reviewing and editing the article, funding acquisition and supervision. Jia Jiang contributed to reviewing and editing the article, funding acquisition and supervision.

Declaration of competing interest

The authors declare that they have no known competing financial interests or personal relationships that could have appeared to influence the work reported in this paper.

Data availability

Data will be made available on request.

Acknowledgments

This work was supported by the National Natural Science Foundation of China (Nos. 81871753, 31972923, 82272570), the Shanghai Talent Development Fund (No. 2021057), and the Shanghai Jiao Tong University Science and Technology Innovation Special Fund (No. 2021JCPT02).

Appendix A. Supplementary data

Supplementary data to this article can be found online at https://doi.org/10.1016/j.mtbio.2023.100749.

References

[1] L.M. Galatz, C.M. Ball, S.A. Teefey, et al., The outcome and repair integrity of completely arthroscopically repaired large and massive rotator cuff tears [J], J. Bone Jt. Surg. Am. Vol. 86A (2) (2004) 219–224.
[2] H.H. Lu, S. Thomopoulos, Functional attachment of soft tissues to bone: development, healing, and tissue engineering [J], Annu. Rev. Biomed. Eng. 15 (2013) 201–226.
[3] F. Fang, Y. Xiao, E. Zelzer, et al., A mineralizing pool of Gli1-expressing progenitors builds the tendon enthesis and demonstrates therapeutic potential [J], Cell Stem Cell 29 (12) (2022) 1669–16684 e6.
[4] G.M. Genin, S. Thomopoulos, The tendon-to-bone attachment: Unification through disarray [J], Nat. Mater. 16 (6) (2017) 607–608.
[5] K.A. Derwin, L.M. Galatz, A. Ratcliffe, et al., Enthesis repair: challenges and opportunities for effective tendon-to-bone healing [J], J Bone Joint Surg Am 100 (16) (2018) e109.
[6] E.D. Bonnevie, R.L. Mauck, Physiology and engineering of the graded interfaces of musculoskeletal junctions [J], Annu. Rev. Biomed. Eng. 20 (2018) 403–429.
[7] C. Zhu, J. Qiu, S. Thomopoulos, et al., Augmenting tendon-to-bone repair with functionally graded scaffolds [J], Adv Healthc Mater 10 (9) (2021), e2002269.
[8] J. Cai, J. Xu, Z. Ye, et al., Exosomes derived from kartogenin-preconditioned mesenchymal stem cells promote cartilage formation and collagen maturation for enthesis regeneration in a rat model of chronic rotator cuff tear [J], Am. J. Sports Med. 51 (5) (2023) 1267–1276.
[9] S. Font Tellado, E.R. Balmayor, M. Van Griensven, Strategies to engineer tendon/ligament-to-bone interface: biomaterials, cells and growth factors [J], Adv. Drug Deliv. Rev. 94 (2015) 126–140.
[10] K. Huang, J. Du, J. Xu, et al., Tendon-bone junction healing by injectable bioactive thermo-sensitive hydrogel based on inspiration of tendon-derived stem cells [J], Mater. Today Chem. 23 (2022), 100720.
[11] J. Xu, W. Su, J. Chen, et al., The effect of antiosteoporosis therapy with risedronate on rotator cuff healing in an osteoporotic rat model [J], Am. J. Sports Med. 49 (8) (2021) 2074–2084.
[12] Z. Chen, M. Jin, H. He, et al., Mesenchymal stem cells and macrophages and their interactions in tendon-bone healing [J], J Orthop Translat 39 (2023) 63–73.
[13] H. Gao, L. Wang, H. Jin, et al., Regulating macrophages through immunomodulatory biomaterials is a promising strategy for promoting tendon-bone healing [J], J. Funct. Biomater. 13 (4) (2022) 243.
[14] J.Y. Sunwoo, C.D. Eliasberg, C.B. Carballo, et al., The role of the macrophage in tendinopathy and tendon healing [J], J. Orthop. Res. 38 (8) (2020) 1666–16675.
[15] J. Ye, C. Xie, C. Wang, et al., Promoting musculoskeletal system soft tissue regeneration by biomaterial-mediated modulation of macrophage polarization [J], Bioact. Mater. 6 (11) (2021) 4096–4109.
[16] Z. Julier, A.J. Park, P.S. Briquez, et al., Promoting tissue regeneration by modulating the immune system [J], Acta Biomater. 53 (2017) 13–28.
[17] K. Zheng, B. Sui, K. Ilyas, et al., Porous bioactive glass micro- and nanospheres with controlled morphology: developments, properties and emerging biomedical applications [J], Mater. Horiz. 8 (2) (2021) 300–335.
[18] M. Vallet-Regi, A.J. Salinas, Mesoporous bioactive glasses for regenerative medicine [J], Mater Today Bio 11 (2021), 100121.
[19] A. Hoppe, N.S. Guldal, A.R. Boccaccini, A review of the biological response to ionic dissolution products from bioactive glasses and glass-ceramics [J], Biomaterials 32 (11) (2011), 2757-2574.
[20] K. Zheng, E. Torre, A. Bari, et al., Antioxidant mesoporous Ce-doped bioactive glass nanoparticles with anti-inflammatory and pro-osteogenic activities [J], Mater Today Bio 5 (2020), 100041.
[21] Q. Wu, L. Hu, R. Yan, et al., Strontium-incorporated bioceramic scaffolds for enhanced osteoporosis bone regeneration [J], Bone Res 10 (1) (2022) 55.
[22] F. Zhao, B. Lei, X. Li, et al., Promoting in vivo early angiogenesis with sub-micrometer strontium-contained bioactive microspheres through modulating macrophage phenotypes [J], Biomaterials 178 (2018) 36–47.
[23] Z. Cai, Y. Li, W. Song, et al., Anti-inflammatory and prochondrogenic in situ-formed injectable hydrogel crosslinked by strontium-doped bioglass for cartilage regeneration [J], ACS Appl. Mater. Interfaces 13 (50) (2021) 59772–59786.
[24] K. Huang, W. Su, X. Zhang, et al., Cowpea-like bi-lineage nanofiber mat for repairing chronic rotator cuff tear and inhibiting fatty infiltration [J], Chem. Eng. J. 392 (2020), 123671.
[25] K. Yu, X. Zhou, T. Zhu, et al., Fabrication of poly(ester-urethane)urea elastomer/gelatin electrospun nanofibrous membranes for potential applications in skin tissue engineering [J], RSC Adv. 6 (77) (2016) 73636–73644.
[26] W. Song, Z. Ma, C. Wang, et al., Pro-chondrogenic and immunomodulatory melatonin-loaded electrospun membranes for tendon-to-bone healing [J], J. Mater. Chem. B 7 (42) (2019) 6564–6575.
[27] S.P. Grogan, A. Barbero, V. Winkelmann, et al., Visual histological grading system for the evaluation of in vitro–generated neocartilage [J], Tissue Eng. 12 (8) (2006) 2141–2149.
[28] S.M. Bolam, Y.E. Park, S. Konar, et al., Obesity impairs enthesis healing after rotator cuff repair in a rat model [J], Am. J. Sports Med. 49 (14) (2021) 3959–3969.
[29] L. Du, C. Qin, H. Zhang, et al., Multicellular bioprinting of biomimetic inks for tendon-to-bone regeneration [J], Adv. Sci. (2023), e2301309.
[30] W. Su, Z. Wang, J. Jiang, et al., Promoting tendon to bone integration using graphene oxide-doped electrospun poly(lactic-co-glycolic acid) nanofibrous membrane [J], Int. J. Nanomed. 14 (2019) 1835–1847.
[31] L. Wang, T. Zhu, Y. Kang, et al., Crimped nanofiber scaffold mimicking tendon-to-bone interface for fatty-infiltrated massive rotator cuff repair [J], Bioact. Mater. 16 (2022) 149–161.
[32] Y. Li, J. Yue, Y. Liu, et al., Strontium regulates stem cell fate during osteogenic differentiation through asymmetric cell division [J], Acta Biomater. 119 (2021) 432–443.
[33] S. Chae, U. Yong, W. Park, et al., 3D cell-printing of gradient multi-tissue interfaces for rotator cuff regeneration [J], Bioact. Mater. 19 (2023) 611–625.
[34] Y.S. Lee, J.Y. Jeong, C.D. Park, et al., Evaluation of the risk factors for a rotator cuff retear after repair surgery [J], Am. J. Sports Med. 45 (8) (2017) 1755–1761.
[35] B.M. Patterson, M.F. Bozoghlian, Modifiable and nonmodifiable risk factors associated with the development of recurrent rotator cuff tears [J], Orthop. Clin. N. Am. 54 (3) (2023) 319–326.
[36] Y.H. Bedeir, A.E. Jimenez, B.M. Grawe, Recurrent tears of the rotator cuff: effect of repair technique and management options [J], Orthop. Rev. 10 (2) (2018) 7593.
[37] C.A. Cummins, G.A. Murrell, Mode of failure for rotator cuff repair with suture anchors identified at revision surgery [J], J. Shoulder Elbow Surg. 12 (2) (2003) 128–133.
[38] N.S. Cho, J.W. Yi, B.G. Lee, et al., Retear patterns after arthroscopic rotator cuff repair: single-row versus suture bridge technique [J], Am. J. Sports Med. 38 (4) (2010) 664–671.
[39] K. Hayashida, M. Tanaka, K. Koizumi, et al., Characteristic retear patterns assessed by magnetic resonance imaging after arthroscopic double-row rotator cuff repair [J], Arthroscopy 28 (4) (2012) 458–464.
[40] L.A. Rossi, S.A. Rodeo, J. Chahla, et al., Current concepts in rotator cuff repair techniques: biomechanical, functional, and structural outcomes [J], Orthop J Sports Med 7 (9) (2019), 2325967119868674.
[41] L. Rossetti, L.A. Kuntz, E. Kunold, et al., The microstructure and micromechanics of the tendon-bone insertion [J], Nat. Mater. 16 (6) (2017) 664–670.
[42] K.L. Moffat, W.H.S. Sun, P.E. Pena, et al., Characterization of the structure-function relationship at the ligament-to-bone interface [J], Proc. Natl. Acad. Sci. U.S.A. 105 (23) (2008) 7947–7952.
[43] A.G. Schwartz, F. Long, S. Thomopoulos, Enthesis fibrocartilage cells originate from a population of Hedgehog-responsive cells modulated by the loading environment [J], Development 142 (1) (2015) 196–206.
[44] E. Zelzer, E. Blitz, M.L. Killian, et al., Tendon-to-bone attachment: from development to maturity [J], Birth Defects Res C Embryo Today 102 (1) (2014) 101–112.
[45] B. Muller, K.F. Bowman Jr., A. Bedi, ACL graft healing and biologics [J], Clin. Sports Med. 32 (1) (2013) 93–109.
[46] S. Roffino, C. Camy, A. Foucault-Bertaud, et al., Negative impact of disuse and unloading on tendon enthesis structure and function [J], Life Sci. Space Res. 29 (2021) 46–52.
[47] P.T. Jensen, K.L. Lambertsen, L.H. Frich, Assembly, maturation, and degradation of the supraspinatus enthesis [J], J. Shoulder Elbow Surg. 27 (4) (2018) 739–750.
[48] J. Pajarinen, T. Lin, E. Gibon, et al., Mesenchymal stem cell-macrophage crosstalk and bone healing [J], Biomaterials 196 (2019) 80–89.
[49] T.L. Fernandes, A.H. Gomoll, C. Lattermann, et al., Macrophage: a potential target on cartilage regeneration [J], Front. Immunol. 11 (2020) 111.
[50] D.S. Amarasekara, H. Yun, S. Kim, et al., Regulation of osteoclast differentiation by cytokine networks [J], Immune Netw 18 (1) (2018) e8.
[51] J.H. Kim, H.M. Jin, K. Kim, et al., The mechanism of osteoclast differentiation induced by IL-1 [J], J. Immunol. 183 (3) (2009) 1862–1870.
[52] Y. Zhu, H. Liang, X. Liu, et al., Regulation of macrophage polarization through surface topography design to facilitate implant-to-bone osteointegration [J], Sci. Adv. 7 (14) (2021), eabf6654.
[53] J. Zou, W. Yang, W. Cui, et al., Therapeutic potential and mechanisms of mesenchymal stem cell-derived exosomes as bioactive materials in tendon-bone healing [J], J. Nanobiotechnol. 21 (1) (2023) 14.
[54] Z. Li, Q. Li, K. Tong, et al., BMSC-derived exosomes promote tendon-bone healing after anterior cruciate ligament reconstruction by regulating M1/M2 macrophage polarization in rats [J], Stem Cell Res. Ther. 13 (1) (2022) 295.
[55] Y. Li, X. Guo, S. Dong, et al., A triple-coated ligament graft to facilitate ligament-bone healing by inhibiting fibrogenesis and promoting osteogenesis [J], Acta Biomater. 115 (2020) 160–175.
[56] A.R. Farmani, M.A. Salmeh, Z. Golkar, et al., Li-doped bioactive ceramics: promising biomaterials for tissue engineering and regenerative medicine [J], J. Funct. Biomater. 13 (4) (2022) 162.

[57] S. Gupta, S. Majumdar, S. Krishnamurthy, Bioactive glass: a multifunctional delivery system [J], J. Contr. Release 335 (2021) 481–497.
[58] M. Fan, W. Liu, C. Fan, et al., Ce and Se co-doped MBG/SA/HLC microgel bone powder for repairing tumor bone defects [J], Nano Res. 16 (2022) 746–756.
[59] F. Kurtuldu, H. Kaňková, A.M. Beltrán, et al., Anti-inflammatory and antibacterial activities of cerium-containing mesoporous bioactive glass nanoparticles for drug-free biomedical applications [J], Materials Today Bio 12 (2021), 100150.
[60] S.G. Dahl, P. Allain, P.J. Marie, et al., Incorporation and distribution of strontium in bone [J], Bone 28 (4) (2001) 446–453.
[61] Z. Xu, X. Qi, M. Bao, et al., Biomineralization inspired 3D printed bioactive glass nanocomposite scaffolds orchestrate diabetic bone regeneration by remodeling micromilieu [J], Bioact. Mater. 25 (2023) 239–255.
[62] C. Deng, H. Zhu, J. Li, et al., Bioactive scaffolds for regeneration of cartilage and subchondral bone interface [J], Theranostics 8 (7) (2018) 1940–1955.
[63] P. Hu, J. Du, S. Zhang, et al., Oral administration of strontium gluconate effectively reduces articular cartilage degeneration through enhanced anabolic activity of chondrocytes and chondrogenetic differentiation of mesenchymal stromal cells [J], Biol. Trace Elem. Res. 193 (2) (2020) 422–433.
[64] Y. Li, M. Chen, J. Yan, et al., Tannic acid/Sr(2+)-coated silk/graphene oxide-based meniscus scaffold with anti-inflammatory and anti-ROS functions for cartilage protection and delaying osteoarthritis [J], Acta Biomater. 126 (2021) 119–131.
[65] X. Dong, J. Chang, H. Li, Bioglass promotes wound healing through modulating the paracrine effects between macrophages and repairing cells [J], J. Mater. Chem. B 5 (26) (2017) 5240–5250.
[66] N.H. Lee, M.S. Kang, T.H. Kim, et al., Dual actions of osteoclastic-inhibition and osteogenic-stimulation through strontium-releasing bioactive nanoscale cement imply biomaterial-enabled osteoporosis therapy, J]. Biomaterials 276 (2021), 121025.
[67] W. Qiao, D. Pan, Y. Zheng, et al., Divalent metal cations stimulate skeleton interoception for new bone formation in mouse injury models [J], Nat. Commun. 13 (1) (2022) 535.
[68] H. Yu, Y. Liu, X. Yang, et al., Strontium ranelate promotes chondrogenesis through inhibition of the Wnt/beta-catenin pathway [J], Stem Cell Res. Ther. 12 (1) (2021) 296.
[69] C. Wang, B. Chen, W. Wang, et al., Strontium released bi-lineage scaffolds with immunomodulatory properties induce a pro-regenerative environment for osteochondral regeneration [J], Mater Sci Eng C Mater Biol Appl 103 (2019), 109833.
[70] Y. Wei, X. Yun, Y. Guan, et al., Wnt3a-Modified nanofiber scaffolds facilitate tendon healing by driving macrophage polarization during repair [J], ACS Appl. Mater. Interfaces 15 (7) (2023) 9010–9023.
[71] J. Cai, J. Liu, J. Xu, et al., Constructing high-strength nano-micro fibrous woven scaffolds with native-like anisotropic structure and immunoregulatory function for tendon repair and regeneration [J], Biofabrication 15 (2) (2023).
[72] Q.Q. Yang, L. Zhang, Y.L. Zhou, et al., Morphological changes of macrophages and their potential contribution to tendon healing [J], Colloids Surf. B Biointerfaces 209 (2022), 112145.
[73] R. Yang, G. Li, C. Zhuang, et al., Gradient bimetallic ion–based hydrogels for tissue microstructure reconstruction of tendon-to-bone insertion [J], Sci. Adv. 7 (26) (2021), eabg3816.